Mon. Not. R. Astron. Soc. **377,** 759–786 (2007) doi:10.1111/j.1365-2966.2007.11647.x

Spatially resolved spectroscopy of early-type galaxies over a range in mass⋆

Patricia Sánchez-Blázquez,[1,2,3]† Duncan A. Forbes,[3] Jay Strader,[4] Jean Brodie[4] and Robert Proctor[3]

[1]*University of Central Lancashire, Centre for Astrophysics, Preston PR1 2HE*
[2]*Laboratoire d'Astrophysique, École Polytechnique Fédérale de Lausanne (EPFL), Observatoire, 1290 Sauverny, Switzerland*
[3]*Centre for Astrophysics and Supercomputing, Swinburne University of Technology, Hawthorn, Victoria 3122, Australia*
[4]*UCO/Lick Observatory, University of California, Santa Cruz, CA 95064, USA*

Accepted 2007 February 19. Received 2007 February 4; in original form 2006 October 31

ABSTRACT

Long-slit spectra have been obtained with the Keck telescope for a sample of 11 early-type galaxies covering a wide range in luminosity and hence mass. Rotation velocity and velocity dispersions, together with 19 Lick line-strength gradients have been measured, to, on average, two effective radii. Stellar population models taking into account the effect of the non-solar chemical composition have been used to derive ages, metallicities and α/Fe abundances along the radius. We find that line-strength gradients are due mainly to variations of the total metallicity with the radius. One galaxy out of 11 shows very strong age gradients, with a young central component, while the age gradient for the rest of the sample is very shallow or consistent with zero. We also find small variations in the [α/Fe] ratio with radius. Contrary to what is expected in simple collapse models, galaxies show both positive and negative [α/Fe] profiles. This rules out a solely inside-out, or outside-in, formation mechanism for all early-type galaxies. We do not find a correlation between the metallicity and the [α/Fe] gradients, and the local metallicity is not correlated with the local velocity dispersion for all the galaxies of our sample, which rules out scenarios where the delay in the onset of the galactic winds is the *only* mechanism producing the metallicity gradients. We found that metallicity gradients are correlated with the shape of the isophotes and the central mean age and metallicity of the galaxies, for galaxies younger than $\sim$10 Gyr. We show that the correlation between the gradients and the central values is not due to the correlation of the errors and indicates that the same process that shaped the gradient, also modified the structural parameters of the galaxies and triggered star formation in their centres. This strongly supports the merger scenario for the formation of these systems, where the degree of dissipation during those mergers increases as the mass of the progenitor galaxies decreases. Finally, we also find a dichotomy in the plane grad [α/Fe]–[α/Fe] between galaxies with velocity dispersions below and above $\sim$200 km s^{-1}, which requires confirmation with larger samples.

Key words: galaxies: abundances – galaxies: elliptical and lenticular, cD – galaxies: evolution – galaxies: formation – galaxies: kinematics and dynamics.

1 INTRODUCTION

The formation and evolution of massive, early-type galaxies constitutes a long-standing and crucial problem in cosmology. In all hierarchical clustering models within a Λ-dominated cold dark matter (ΛCDM) cosmology, the massive early-type galaxies seen now are expected to have formed through the merger of smaller galaxies over time (e.g. White & Frenk 1991; Somerville & Primack 1999; Cole et al. 2000; de Lucia et al. 2006). These models have found strong

⋆The data presented herein were obtained at the W.M. Keck Observatory, which is operated as a scientific partnership among the California Institute of Technology, the University of California and the National Aeronautics and Space Administration. The observatory was made possible by the generous financial support of the W.M. Keck Foundation.
†E-mail: psanchez-blazquez@uclan.ac.uk

support in the recent studies based on the COMBO-17 and DEEP2 surveys which show that the number density of red galaxies has increased since redshift $z = 1$ (Bell et al. 2004; Faber et al. 2005). This is true even for the more massive galaxies on the red sequence (although see Cimatti, Daddi & Renzini 2006, for another point of view).

However, most of the studies of the evolution of the Fundamental Plane and colour–magnitude relation with redshift are compatible with an epoch of formation of the stars in these galaxies at $z > 2$ and a passive evolution since then (e.g. Kelson et al. 2000; Gebhardt et al. 2003; Fritz et al. 2005), at least for the brightest galaxies. Fainter galaxies may have formed a large percentage of their stars at later times (di Serego Alighieri et al. 2005; Holden et al. 2005; van der Wel et al. 2005). If, as usually assumed in the hierarchical models, mergers between galaxies trigger star formation, we would expect elliptical galaxies to show a spread in their ages, and, therefore, in their colours, spreading the scatter of the colour–magnitude and Fundamental Plane correlations, contrary to what it is observed. This problem for the models may be partially solved if any new stars formed are more metal rich, as both, an increase in age and metallicity produce a reddening of the colours (see e.g. Faber, Worthey & González 1992; Ferreras, Charlot & Silk 1999). Furthermore, in the last few years there have been several studies showing that mean age (as derived with single stellar population models) of more massive early-type galaxies is larger than the one in the less massive ones (e.g. Caldwell, Rose & Concannon 2003; Nelan et al. 2005; Sánchez-Blázquez et al. 2006c) which would indicate an antihierarchical formation of the stars in the galaxies. Again, the antihierarchical formation of stars can be reconciled with the hierarchical formation of structures decoupling the epoch of the star formation from the epoch of the mass assembly. In this scenario, there is a systematic decrease, with increasing mass, of the relative amount of dissipation (and, therefore, star formation) experienced by the baryonic mass component when they assemble (e.g. de Lucia et al. 2006).

Moreover, a successful scenario of galaxy formation must reproduce not only the photometric properties of the galaxies but also their structural parameters. Normal and low-luminosity elliptical galaxies rotate rapidly, are nearly isotropic, show discy-distorted isophotes and cuspy inner profiles. On the contrary, giant ellipticals are essentially non-rotating, show anisotropic dynamics, *core* inner profiles and boxy isophotes (Kormendy & Bender 1996). The properties of the former can be explained in dissipational mergers, while the latter are recovered successfully with dissipationless mergers.

One way to test this prediction is to study the stellar population gradients in early-type galaxies. The stellar population gradients do not only give information about the formation epoch of the stars in the galaxies, but also about the formation process, as gas dissipation and mergers affect the gradients in different ways (e.g. Larson 1975; White 1980; Mihos & Hernquist 1994; Angeletti & Giannone 2003; Kobayashi 2004). The correlation of the derived stellar population parameters (age, metallicity, abundances ratios) with other global galaxy properties could offer, in principle, invaluable information to determine how the formation and subsequent evolution of early-type galaxies has occurred.

For example, in the classical models of monolithic collapse (Eggen, Lynden-Bell & Sandage 1962; Larson 1974a; Carlberg 1984; Arimoto & Yoshii 1987; Gibson 1997), stars form in all regions during the collapse and remain in their orbits with little movement inward, whereas gas dissipates into the centre, being continuously enriched by the evolving stars. Therefore, stars formed in the centre are predicted to be more metal rich than those in the outer regions. On the other hand, as a consequence of the continuous enrichment by evolving stars, the centres are predicted to be less α enhanced than the external parts, unless the collapse is extremely short in time. To obtain the high central values of α/Fe measured in early-type galaxies, the duration of the collapse is limited to $\sim$1 Gyr (Arimoto & Yoshii 1987; Thomas 1999), therefore, null or very small age gradients are expected within this picture. As the degree of dissipation in these models is controlled by the potential well, a strong correlation between the metallicity gradient and the mass of the galaxies is also predicted. Supernova-driven galactic winds may also help to shape the abundances gradients (Mathews & Baker 1971; Larson 1974b; Arimoto & Yoshii 1987; Franx & Illingworth 1990; Gibson 1997; Martinelli, Matteucci & Colafrancesco 1998). These winds, initiated when the energy injected by supernovae into the interstellar medium matches that of the binding energy of the galaxies, act to evacuate the galaxy of gas, thereby eliminating the fuel necessary for star formation. As external parts have shallower potential wells, galactic winds develop earlier than in the central regions, where the star formation and the subsequent chemical enrichment last longer. This mechanism would also lead to positive α/Fe gradients (Martinelli, Matteucci & Colafrancesco 1998; Pipino, Matteucci & Chiappini 2006).

Predictions of the resultant metallicity gradient of a merger remnant are more complicated, as those depend on a large number of free parameters. In general, numerical simulations suggest that dissipationless mergers lead to a flattening of metallicity gradients (White 1980). However, numerical simulations with gas suggest that during the merger a significant gas fraction migrates toward the central regions of the merging galaxies resulting in a starburst (Barnes & Hernquist 1991). These episodes of star formation can also produce metallicity and age gradients (Mihos & Hernquist 1994). If star formation is triggered in the centre of the galaxy due to the merger, [α/Fe] gradients can be both positive or negative depending on the duration of the burst and the original abundance pattern of the gas (see e.g. Thomas, Greggio & Bender 1999; Pipino & Matteucci 2006). On the other hand, the degree of dissipation and the ratio between the masses of the two merging systems produce differences in the kinematics, shape of the isophotes and other properties of the final remnants (see e.g. Bekki & Shioya 1997; Naab, Jesseit & Burkert 2006a).

Several authors have investigated the variation in the colours (e.g. Vader et al. 1988; Peletier et al. 1990; Silva & Bothun 1998; Saglia et al. 2000; Tamura & Ohta 2000, 2003; Tamura et al. 2000; Hinkley & Im 2001; Idiart, Michard & de Freitas Pacheco 2002; La Barbera et al. 2004, 2005; Menanteau et al. 2004; de Propris et al. 2005; Wu et al. 2005) and line-strength indices (e.g. Spinrad et al. 1971; Cohen 1979; Franx & Illingworth 1990; Gorgas, Efstathiou & Aragón-Salamanca 1990; Davidge 1992; Carollo, Dazinger & Buson 1993; Davies, Sadler & Peletier 1993; González 1993; Fisher, Franx & Illingworth 1996; Mehlert et al. 2003; Proctor et al. 2005; Kuntschner et al. 2006; Sánchez-Blázquez, Gorgas & Cardiel 2006d) with radius in early-type galaxies, and the results so far appear to be contradictory in many cases: for example, Peletier et al. (1990) found that for galaxies brighter than $M_B = -21$ the colour gradient gets flatter with luminosity, while the contrary is seen for galaxies fainter than this magnitude. However, Tamura & Ohta (2003) found the opposite trend in the relation of their colour gradients with magnitude.[1] Carollo et al. (1993) found a correlation

[1] The colour analysed by Peletier et al. (1990) was $U - R$ while Tamura & Ohta (2003) present their results using $B - R$.

between the Mg_2 gradient and the magnitude, central velocity dispersion and mass, but only for faint galaxies, while this correlation has not been confirmed by other studies (e.g. Kobayashi & Arimoto 1999). Other uncertain results include the existence of a correlation between the line-strength index gradients and central values found by some authors (e.g. González & Gorgas 1995; Kuntschner et al. 2006; Sánchez-Blázquez et al. 2006d) but not by others (e.g. Kobayashi & Arimoto 1999; Mehlert et al. 2003).

The lack of agreement between studies is partially due to the high signal-to-noise ratio (S/N) necessary to measure metallicity gradients with accuracy. In this paper we make the first attempt to overcome this limitation, presenting very high quality data allowing for the determination of line-strength gradients in a sample of 11 early-type galaxies spanning a wide range in luminosity. In Section 2 we introduce the sample and the observations, together with a description of the data reduction. Section 3 presents the rotation curves and the velocity dispersion (σ) profiles. Section 4 and 5 describe the measurement of the spectroscopic indices and the transformation of those into age, metallicity and α-enhancement gradients, respectively. In Section 6, we perform a brief analysis of the central indices. Sections 7.1, 7.2 and 7.3 show the analysis of the age, metallicity and [E/Fe] gradients, and their correlation with other global parameters of the galaxies. Section 8 presents the correlation between the local metallicity and the local σ, while in Section 9 we discuss our results.

2 THE SAMPLE: OBSERVATIONS AND DATA REDUCTION

The sample consists of 11 galaxies, covering a wide range in luminosity, extracted from the field, poor groups and the Virgo cluster. Table 1 summarizes the main properties of the sample, and Appendix A includes an enhanced discussion of each galaxy's properties.

2.1 Observations and data reduction

2.1.1 Observations

The observations were made using Low Resolution Imaging Spectrograph (Oke et al. 1995) in long-slit mode on the Keck II telescope. All 11 galaxies were observed on a two-night run in 2005 February 8–9. Two 600-s exposures were taken for each galaxy except for NGC 4472 where two exposures of 600 and 300 s were taken. The slit was 175-arcsec long and 1.5-arcsec wide, and was oriented along the major axis of the galaxies. We use the 400 line mm^{-1} grism blazed at 3400 Å. This instrumental set-up gives a spectral resolution of ∼8.0 Å [full width at half-maximum (FWHM)] and a dispersion of 1.09 Å $pixel^{-1}$. The total wavelength coverage is 3110–5617 Å. A total of five stars belonging to both the Lick Observatory Image Dissector Scanner (Lick/IDS) stellar library (Gorgas et al. 1993; Worthey 1994) and MILES library (Sánchez-Blázquez et al. 2006a) were observed. These stellar templates though, we observed with a different grating than the galaxies and, therefore, were only used to measure the seeing during the observations and to flux calibrate the spectra.

2.1.2 Data reduction

The standard data reduction procedures (bias subtraction, flat-fielding, cosmic-ray removal, wavelength calibration, sky subtraction and flux calibration) were performed with REDUCEME (Cardiel 1999). This reduction package allows a parallel treatment of data and error frames and, therefore, produces an associate error spectrum for each individual data spectrum. After the bias subtraction, the pixel-to-pixel sensitivity variations were removed (using flat-field exposures of a tungsten calibration lamp).

Prior to the wavelength calibration, arc frames were used to correct from geometrical distortions along the spatial direction (C-distortion) in the images. This correction guarantees alignment errors to below 0.1 pixel. Spectra were converted to a linear scale using typically 50-arc lines fitted by 3rd–5th order polynomial with rms residuals of 0.1 Å. The spectra were also corrected for geometrical distortions along the spectral direction (S-distortion). To do that we use a routine that finds the maximum corresponding to the centre of the galaxy as a function of wavelength and fits these positions with a low-order polynomial. The spectra are then accordingly displaced using a technique that minimizes the errors due to the discretization of the signal. The typical error in the centring of the object is very small, ∼0.1 pixel (see Cardiel 1999 for details).

Atmospheric extinction was calculated using the extinction curve from the Canada–France–Hawaii Telescope (CFHT) Bulletin, number 19, p. 16 (1998) available through http://www.jach.hawaii.edu/

Table 1. Sample of galaxies. Type: morphological classification from the NED. $r_{\rm eff}$: effective radius from Burstein et al. (1987), with the exception of NGC 3384, from which the effective radius was extracted from the RC3 catalogue. Magnitude: from Hyperleda data base (assuming $H_0 = 70\,{\rm km\,s^{-1}\,Mpc^{-1}}$). Inner profile types are extracted from Lauer et al. (1995) – Ref 1; Rest et al. (2001) – Ref 2; Ravindranath et al. (2001) – Ref 3; Lauer et al. (2005) – Ref 4. $\log(v/\sigma)$*: anisotropy parameter calculated as described in the text. (a4/a) × 100: the values have been taken from Bender et al. (1989) except for the galaxy NGC 2865, where the value is from Reda et al. (2004). Env: environment where the galaxies are located.

Galaxy	Type	$r_{\rm eff}$ (arcsec)	M_B (mag)	Profile	Ref.	$\log(v/\sigma)$*	(a4/a) × 100	Env
NGC 1600	E3	47.5	−22.4	Core	1	−1.495	−0.7	Field
NGC 1700	E4	13.7	−21.9	Power/core	1/4	−0.359	0.4	Group
NGC 2865	E3-4	11.7	−20.8			0.319	1.5	Field
NGC 3377	E5-6	33.7	−19.2	Power, power	1/2	−0.137	1.2	Leo I group
NGC 3379	E1	35.2	−20.6	Core	1	−0.150	0.2	Leo I group
NGC 3384	SB0	24.9	−19.9	Power	1/3	−0.137		Leo I group
NGC 4387	E5	15.4	−17.0	Power	1	−0.240	−1.0	Virgo cluster
NGC 4458	E0-1	26.7	−17.4	Power/core	1/4	−0.154		Virgo cluster
NGC 4464	E3	5.3	−18.0	Power	1	−0.078		Virgo cluster
NGC 4472	E2/S0	104.0	−21.8	Core	1/3	−0.455	−0.3	Virgo cluster
NGC 4551	E	17.7	−17.7	Power	1	−0.298	−0.6	Virgo cluster

UKIRT/astronomy/exts.html. To correct for the effect of interstellar extinction, we used the curve of Savage & Mathis (1979) and values of the colour excess, $E(B-V)$, from NASA/IPAC Extragalactic Database (NED).

Some of the reduction steps, such as sky subtraction, can have a significant impact on the derived gradient. Since galaxy light levels are usually only a few per cent of the sky signal in the outer parts of the galaxies, this process constitutes one of the most important potential sources of systematic errors (see Cardiel, Gorgas & Aragón-Salamanca 1995). Fortunately, our observations were performed in dark time, which reduce the variability of the sky during the exposures and, therefore, improve the accuracy of the correction. One of the main problems to perform a proper sky subtraction is that some of the galaxies are large enough to fill a large part of the data frames, so that a sky spectrum measured at the edges of the frame is contaminated by light from the galaxy. In order to avoid this problem, we offset the centre of the slit from the galaxy centre. This ensures a lower level of contamination, at least in the sky measured at one of the edges of the frames. The sky level was measured at the end of the slit and subtracted from the whole image. To test the error in the sky subtraction we selected the galaxy with a larger effective radii of our sample, NGC 4472 and measured the number of counts that the galaxy contributed in the sky regions. This was done by fitting a de Vaucouleurs profile to the surface brightness profile of the galaxy. The contamination of the galaxy in the selected region was lower than 1 per cent. This contamination produces a negligible effect in the measured indices.

Relative flux calibration of the spectra was achieved using exposures of standard stars. All the calibration curves were averaged and the errors on the indices due to the errors on the flux calibration were estimated by the differences between the indices measured with different curves.

From each full galaxy frame, a final two-dimensional spectrum was created by extracting spectra along the slit, binning in the spatial direction the necessary number of one-dimensional (1D) spectra to guarantee a *minimum* S/N per Å of 50 in the spectral region of the Hβ index, which ensures a maximum relative error for this index of 9 per cent (see Cardiel et al. 1998). Imposing this criteria, we can measure line-strength indices, in most galaxies, at distances from the centre of $r \sim 2r_{\rm eff}$. This S/N at this radius has not been achieved previously.

3 KINEMATIC PROFILES

Radial velocities and velocity dispersions for each spectrum were calculated using MOVEL and OPTEMA algorithms described by González (1993). The MOVEL algorithm (improved version of the classic Fourier quotient method by Sargent et al. 1977) is an iterative procedure in which a galaxy model is processed in parallel to the galaxy spectrum. In this way, a comparison between the input and recovered broadening functions for the model allows one to correct the galaxy power spectrum from any imperfections of the data handling in Fourier space. The main improvement of the procedure is introduced through the OPTEMA algorithm, which is able to overcome the typical template mismatch problem. For each spectrum, 25 star spectra from the MILES library (Sánchez-Blázquez et al. 2006a) were scaled, shifted and broadened according to a first guess of the γ (mean line strength), v (radial velocity) and σ (velocity dispersion) parameters, having into account the difference in spectral resolution between the stellar and the galaxy spectra. The next step is to find the linear combination of the template spectra that best matches the observed galaxy spectrum. This provides a first composite template which is fed into the MOVEL algorithm. The output kinematic parameters were then used to create an improved composite template and the process was iterated until it converged. This iterative approach provides an optimal template while simultaneously computing the radial velocity and velocity dispersion of the galaxy spectrum. In Fig. 1 we show a typical fit between the central spectrum of a galaxy and its corresponding optimal template corrected with the derived kinematic parameters. For each galaxy spectrum, random errors in the derived kinematic parameters were computed by numerical simulations. In each simulation, a bootstrapped galaxy spectrum, calculated from the error spectra provided by the reduction with REDUCEME by assuming Gaussian errors, is fed into the algorithms described above. Errors in the parameters are then calculated as the standard deviations of the different solutions.

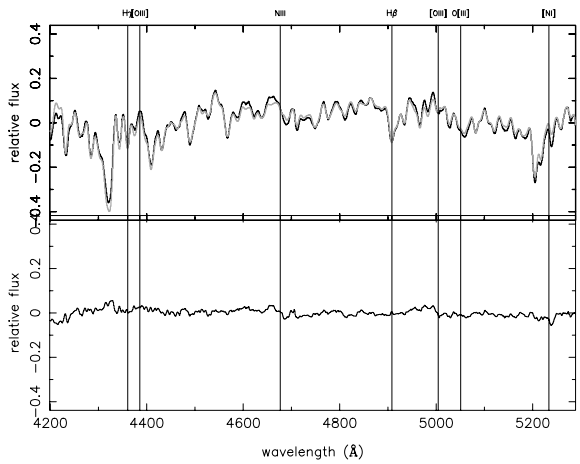

Figure 1. Top panel: final fit of the optimal template corrected with the kinematic parameters (grey line) to the spectrum of the galaxy NGC 4387 (dark line). The bottom panel shows the residuals of this fit. The vertical lines indicate the position of several typical absorption and emission lines.

Fig. 2 shows the kinematic profiles and velocity dispersion profiles for all the galaxies in the sample. Below we analyse the rotation curve and velocity dispersion profile for the individual galaxies.

NGC 1600: very little rotation and high velocity dispersion along the radius.

NGC 1700: clear evidence seen in the profile of the presence of a counter-rotating core, previously found by other authors (Statler, Smecker-Hane & Cecil 1996) and a large rotation at large radii. The velocity dispersion profile shows a depression in the central parts, which indicates that a more rotationally supported component is present at the galaxy centre.

NGC 2865: this galaxy shows also the presence of a kinematically decoupled core with a radius of ∼5 aecsec and a large rotation at larger radii.

NGC 3377: this galaxy shows large rotation in the centre, indicating the possible presence of a central disc. Beyond ∼5 arcsec, the velocity along the radius remains constant.

NGC 3379: this galaxy shows very little rotation.

NGC 3384: the rotation curve indicates that the slit was not perfectly centred during the observations. The velocity dispersion profile shows a depression in the centre.

NGC 4387: the velocity dispersion profile shows a depression in the centre, which may indicate the presence of a stellar disc.

NGC 4458: the kinematic profile in this galaxy indicates that the slit was not perfectly centred in the object. Apart from that the galaxy shows evidence for a kinematically decoupled core.

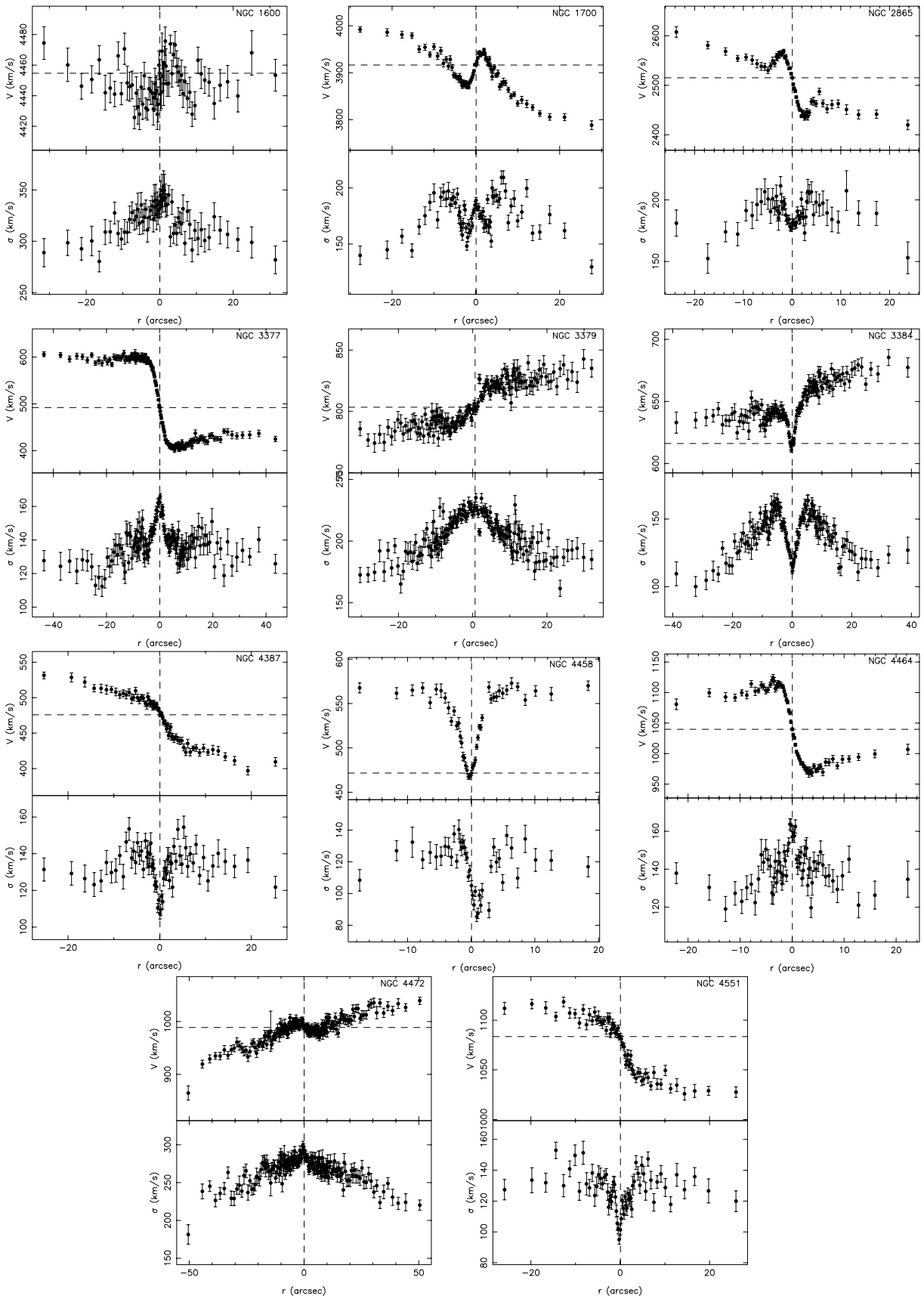

Figure 2. Rotation velocity curves and velocity dispersion profiles for our sample of galaxies.

NGC 4464: this galaxy shows a rotational curve consistent with the presence of a gaseous disc (see also Halliday et al. 2001) with a scalelength of ∼4 arcsec. The rotation curve starts to decrease beyond this radius.

NGC 4472: we detect some indication of a kinematically decoupled structure in the centre of the galaxy, with very little rotation.

NGC 4551: this galaxy shows rotation in the central parts and then the rotation curve is flat at larger radii. The velocity dispersion profile shows a depression in the centre.

We confirm the presence of kinematically decoupled cores in several galaxies: NGC 1700, 2865 and 4458, as previously reported by other studies (Statler, Smecker-Hane & Cecil 1996; Hau, Carter & Balcells 1999; Morelli et al. 2004). Ellipticals with kinematically decoupled cores can originate from dissipative major galaxy mergers between two spirals (Hernquist & Barnes 1991), a spiral and a elliptical (Franx & Illingworth 1988) or by accretion of small satellites via dynamical friction (Kormendy 1984), although the decoupled subsystems are often dynamically colder than expected from purely stellar satellite accretion (Franx & Illingworth 1988; Bender & Surma 1995). Recent studies favour major mergers to form kinematically decoupled structures (Jesseit et al. 2007). These kinematically decoupled structures, however, cannot be formed in mergers without dissipation.

We also found that for the galaxies NGC 3384 and 4458 the slit was slightly offset from the centre of the galaxy. In principle, one concern is that this could affect the gradients. However, the line-strength indices gradients of these two galaxies are compared with the ones derived by the SAURON group (Kuntschner et al. 2006) in Appendix C, and they are very similar. Therefore, we consider that the gradients we are measuring are not very dissimilar to the ones we would have obtained with the slit perfectly centred in the galaxies.

4 LINE-STRENGTH INDICES

In each individual spectrum we measured a total of 15 Lick/IDS indices (from CN_1 to Fe5335; Trager et al. 1998), the D4000 break (Bruzual 1983) and the four higher order Balmer lines $H\delta_A$, $H\delta_F$, $H\gamma_A$ and $H\gamma_F$ defined by Worthey & Ottaviani (1997). In order to compare the measured indices with stellar population models using the fitting functions obtained with the Lick/IDS stellar library (Gorgas et al. 1993; Worthey et al. 1994), the data have to be transformed into the Lick/IDS spectrophotometric system. The transformation into the Lick/IDS system compensates for two different effects. The first effect is the instrumental and Doppler broadening. Before measuring the indices on the spectra, they have to be degraded to the resolution of the Lick/IDS library and the indices have to be corrected for the internal motions of the stars. The usual method to perform this correction is to convolve the stellar spectra with different broadening functions of different velocity dispersions and use a polynomial expansion to describe the variation of a given line index as a function of the input velocity dispersion. However, the variation of a given line index with velocity dispersion depends on the strength of the index itself. (see, for example, appendix B2 in Kuntschner 2000). Therefore, by assuming a single polynomial we are introducing systematic errors that can affect the relation of the indices with the velocity dispersion. To avoid these problems, we perform the broadening corrections following the method described in Kelson et al. (2006). The corrected line-strength indices are obtained as follows:

$$I_{\rm corr} = I_{\rm G} + \left(I_{\rm T_{IDS}} - I_{B(\sigma)\rm oT}\right), \quad (1)$$

where $I_{\rm G}$ is the index measured directly on the galaxy spectrum, $I_{B(\sigma)\rm oT}$ the index measured from the optimal template spectrum (obtained in the computation of the velocity dispersions, see Section 3) broadened to the instrumental resolution and to the velocity dispersion of the galaxy and $I_{\rm T_{IDS}}$ is the index measured on the optimal template spectrum with a velocity dispersion of zero and convolved to the resolution of the Lick/IDS system (Worthey & Ottaviani 1997).

The second effect that has to be corrected is the small systematic differences that appear when the indices measured on the Lick stars and in flux-calibrated stars are compared. These small offsets are partially due to the differences in the continuum shape, as Lick/IDS stars are not flux calibrated, although these differences do not explain the offsets of all indices (see e.g. Worthey & Ottaviani 1997). The usual procedure to perform this correction is to observe, with the same instrumental configuration as the galaxies, stars in common with the Lick/IDS library and compare the indices measured in them (after degrading the spectra to match the Lick/IDS resolution) with the indices measured on the Lick spectra. However, we did not observe stars with the same instrumental configuration as the galaxies. Therefore, we derived these offsets by comparing the indices of 10 galaxies in common with Trager et al. (1998), which were observed with the same instrumental set-up as the Lick/IDS library. In order to avoid artificial offsets due to line-strength gradients in galaxies, we extracted the spectra in an aperture of $4 \times 1.5\,\mathrm{arcsec}^2$, very similar to the one in Trager et al. (1998) ($4 \times 1.4\,\mathrm{arcsec}^2$).

However, Trager et al. (1998) do not measure the Hδ and Hγ indices. To determine the offsets in the high-order Balmer lines we compare the indices of five galaxies in common with Sánchez-Blázquez (2004). We selected the measurements within an aperture of $2 \times 4\,\mathrm{arcsec}^2$, which is the most similar to the $4 \times 1.4\,\mathrm{arcsec}^2$ aperture used by Trager et al. A detailed comparison is shown in Appendix B. The final offsets are listed in Table 2.

Table 2. Comparison of the Lick/IDS line-strength indices measured in this work with Trager et al. (1998). Offset: mean offsets to transform into the Lick system. rms: root mean square deviations of the comparison. rms(exp): rms expected by the errors. z: z parameter to determine the statistical significance of the offset. When $z < 1.9$ (equivalent to a difference lower than 3σ) we consider the offset is not significant and set it as zero.

Index	Offset	rms	rms(exp)	z
$H\delta_A$	0.000	0.099	0.089	0.52
$H\delta_F$	0.000	0.084	0.056	0.86
CN_1	−0.029	0.013	0.013	2.75
CN_2	−0.039	0.017	0.016	2.72
Ca4227	−0.228	0.139	0.224	2.64
G4300	0.000	0.356	0.267	1.47
$H\gamma_A$	0.380	0.124	0.085	1.92
$H\gamma_F$	0.533	0.060	0.050	1.99
Fe4383	−0.272	0.328	0.478	1.97
Ca4455	0.000	0.165	0.193	0.96
Fe4531	0.000	0.288	0.318	1.06
C4668	−0.571	0.434	0.480	2.43
$H\beta$	0.000	0.146	0.163	1.07
Fe5015	0.000	0.611	0.413	1.27
Mg_1	0.000	0.008	0.011	1.27
Mg_2	0.011	0.008	0.012	2.50
Mgb	−0.349	0.133	0.181	2.82
Fe5270	−0.112	0.210	0.174	1.47
Fe5335	−0.332	0.201	0.213	2.60

4.1 Emission-line correction

A large percentage of early-type galaxies show small amounts of gas. Some line-strength indices are affected by these emission lines. In particular, this is the case of Hβ, Fe5015 and Mgb. Before measuring line-strength indices this emission has to be removed. To measure the flux of the emission lines we used the routine GANDALF (Sarzi et al. 2006). This routine fits simultaneously both the stellar spectrum and emission lines, treating the emission lines as additional Gaussian templates. For the stellar templates, we use synthetic stellar energy distributions from Vazdekis et al. (in preparation) based on the MILES stellar library (Sánchez-Blázquez et al. 2006a). Our detection limit is 0.3 Å for [O III]λ5007 and [N I]λ5200, and 0.25 Å for Hβ (see Sarzi et al. 2006, for details on how to calculate this threshold). NGC 1700, 2865, 3377, 3379, 3384 show the presence of weak emission lines above our detection limit. The emission spectra were subtracted to the galaxy spectra and indices measured in the emission-free spectra.

In order to check the reliability of our line-strength gradients we have compared the derived line-strength indices with the ones derived by other authors, in particular, with the studies by Fisher et al. (1996) and Kuntschner et al. (2006). The results of this comparison can be found in Appendix C. In general, the agreement is very good, although none of these studies reaches the same distance from the galaxy centres as the present study.

5 STELLAR POPULATION PARAMETERS GRADIENTS

We derive single stellar population (SSP)-equivalent parameters age, [Fe/H] and α-abundance ratios for all the galaxies of the sample using the χ^2-minimization technique detailed in Proctor & Sansom (2002), Proctor, Forbes & Beasley (2004b) and Proctor et al. (2004a). The technique involves the comparison of as many indices as possible to SSP models. In the method described by Proctor et al. (2004b,a) the indices which significantly deviate by more than 3σ are clipped from the fit and χ^2 is recalculated. However, in this study, we have preferred to obtain the stellar population parameters with the same indices for all the galaxies in order to obtain homogeneous ages and abundances, although the results do not change if we clip the deviating indices (see below). In particular, we used 19 indices, including all Lick/IDS and Worthey & Ottaviani (1997) indices.

We adopted the SSP models of Thomas, Maraston & Bender (2003, hereafter TMB03) and Thomas, Maraston & Korn (2004) for the extension to the higher order Balmer lines. These models include the effect that a variation in the [α/Fe] ratios produces in the Lick indices. To do that the authors used the new response functions by Korn, Maraston & Thomas (2005), as opposed to the widely used response functions by Tripicco & Bell (1995). An important improvement of the Korn et al. (2005) response function over the ones by Tripicco & Bell (1995) is the treatment of the element carbon. Houdashelt et al. (2002) pointed out that enhancing the abundance of C by +0.3 (which is the factor Tripicco & Bell fitting functions use) brings the C/O ratio very close to unity producing a carbon star. Worthey (2004) noticed that the response functions of Tripicco & Bell (1995) are overestimating the sensitivity of C4668 to C by not taking this effect into account. The Korn et al. (2005) response functions deal with this problem by computing the sensitivity of indices to C by increasing the C abundance by only +0.15 dex. The α enhancement is parametrized in these models by [E/Fe]; the abundance ratio of the α elements O, Ne, Mg, Si, S, Ar, Ca and Ti plus the elements N and Na (see the original references for details).

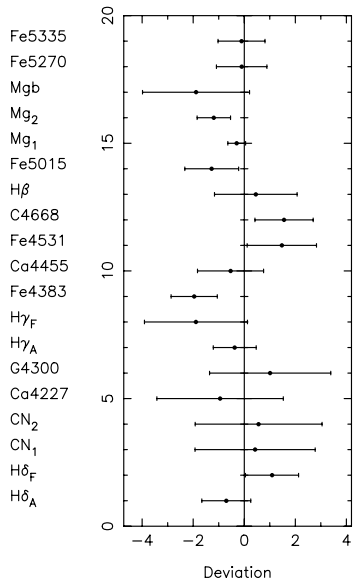

Figure 3. Average deviation in units of error (i.e. χ) of the measured indices from the indices corresponding to the best fitting. Error bars represent the scatter in the deviation.

Residuals to the best fitting (observed value minus best-fitting value expressed in terms of the index errors) for all the galaxies are summarized in Fig. 3. The points represent the average deviation from the best-fitting values while the errors bars show the rms for all the points along the radius. As can be seen, the mean differences between the fitted and the measured errors are very small, confirming the reliability of the fitting procedure.

Figs 4, 5 and 6 show the age, metallicity and [E/Fe] profiles for all the galaxies in our sample. We have to remind the reader that those values of age, metallicity and [E/Fe] are SSP-equivalent parameters. If galaxies experience a star formation history more complicated than a single, instantaneous burst, those values have to be carefully interpreted: for example, if a galaxy has experience two burst of star formation separated in time, the SSP-age would be biased toward the age of the youngest stars, while the SSP-metallicity would be closer to the metallicity of the old population (although this depends, of course, of the mass fraction of the bursts, see e.g. Serra & Trager 2007, for a detailed analysis).

To quantify the profiles we perform a linear fit weighting with the errors in the y direction and excluding the points from the centre within the diameter of the seeing disc to avoid seeing effects. The extent of the seeing disc (FWHM of the point spread function) was taken from the measurements performed by the Mauna Kea seeing monitor, but the measurements were checked by measuring the FWHM of the point spread functions on observed standard stars. The points excluded from the fit are represented with open symbols. For completeness, we have performed also a linear fit on the age profile of the galaxy NGC 3377, despite this profile being clearly non-linear. The errors in the gradients were calculated as the unbiased standard deviation from the fit. Table 3 shows the derived gradients of age, [Z/H] and [E/Fe].

5.1 Checking the reliability of the stellar population gradients

One of the major problems of using a large number of indices to derive stellar population parameters by χ^2 minimization is related to the zero-point of the models. Although we have added suitable

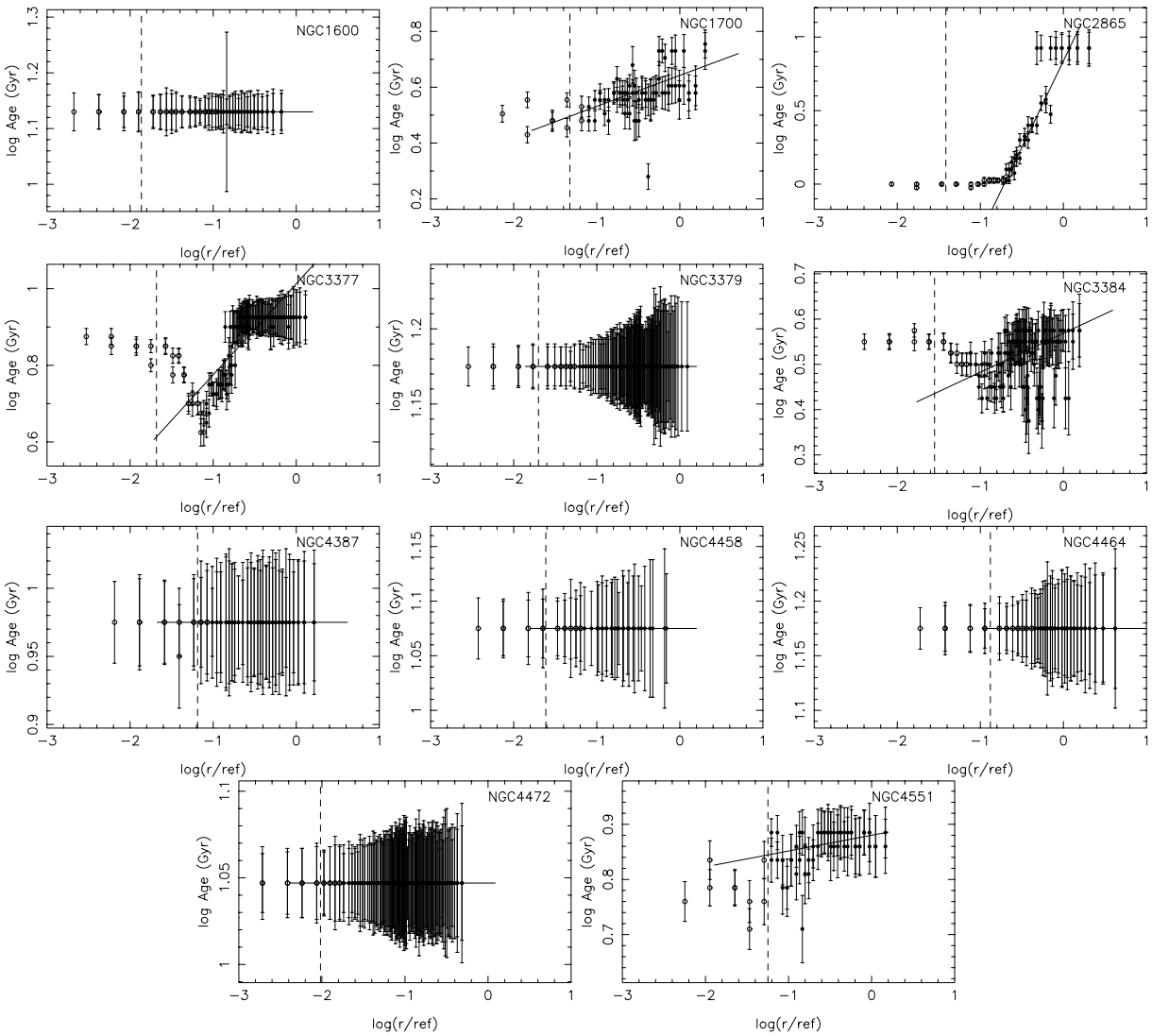

Figure 4. SSP-equivalent-age profiles for the sample of galaxies calculated with TMB03 models using a set of 19 different Lick indices. Dashed lines indicate the extent of the seeing disc. Solid lines represent a linear fit to the data weighting with errors in the y direction. Open symbols have been excluded from the fit (see text for details).

offsets to transform our data into the Lick/IDS spectrophotometric system, the models have problems reproducing some of the measured indices for Galactic globular clusters (e.g. TMB03). The same problem has been observed in elliptical galaxies where it has been also shown that the age and metallicity depend on the index used to measure those parameters (e.g. Peletier et al. 1990; Faber et al. 1992; Vazdekis et al. 2001; TMB03; Sánchez-Blázquez et al. 2006c).

Most of these differences, but not all, can be attributed to peculiar abundances ratios in the Galactic globular clusters and elliptical galaxies (TMB03). In fact, TMB03 showed that part of the problem is solved with the inclusion of non-solar [α/Fe] abundances in the models but, certainly, this is still an issue when one wishes to use a large number of indices with different sensitivities to different chemical species as (1) some other elements apart from the ones considered in the models may have abundances ratios different from solar and (2) because it may be the case that not all the α elements are equally enhanced, as seen, for example, in the Galactic bulge (Lecureur et al. 2007).

Kelson et al. (2006) treated this problem by recalibrating the stellar population models. To do that they used a reference galaxy and assigned to it an approximate age, metallicity and [α/Fe]. They derived offsets in all the indices so the final indices coincide with the values given by the models for the selected stellar population parameters. They applied these offsets to all the galaxies in their sample. This study was the first to take the effect of the zero-point into account in the derivation of ages and metallicities using a large number of indices. However, their approach assumes that the offsets are the same for all the galaxies, while, if the offset is due to differences, for example, in the chemical abundance ratios not considered in the models, this assumption presumably would not be true, as the chemical composition is different for galaxies of different masses. Furthermore, if galaxy stellar populations are not suitably described by means of SSP models, the age and metallicities measured with different indicators might be different, simply because the weight of different stars to different regions of the spectra is different (e.g. Sánchez-Blázquez et al. 2006c; Schiavon 2006).

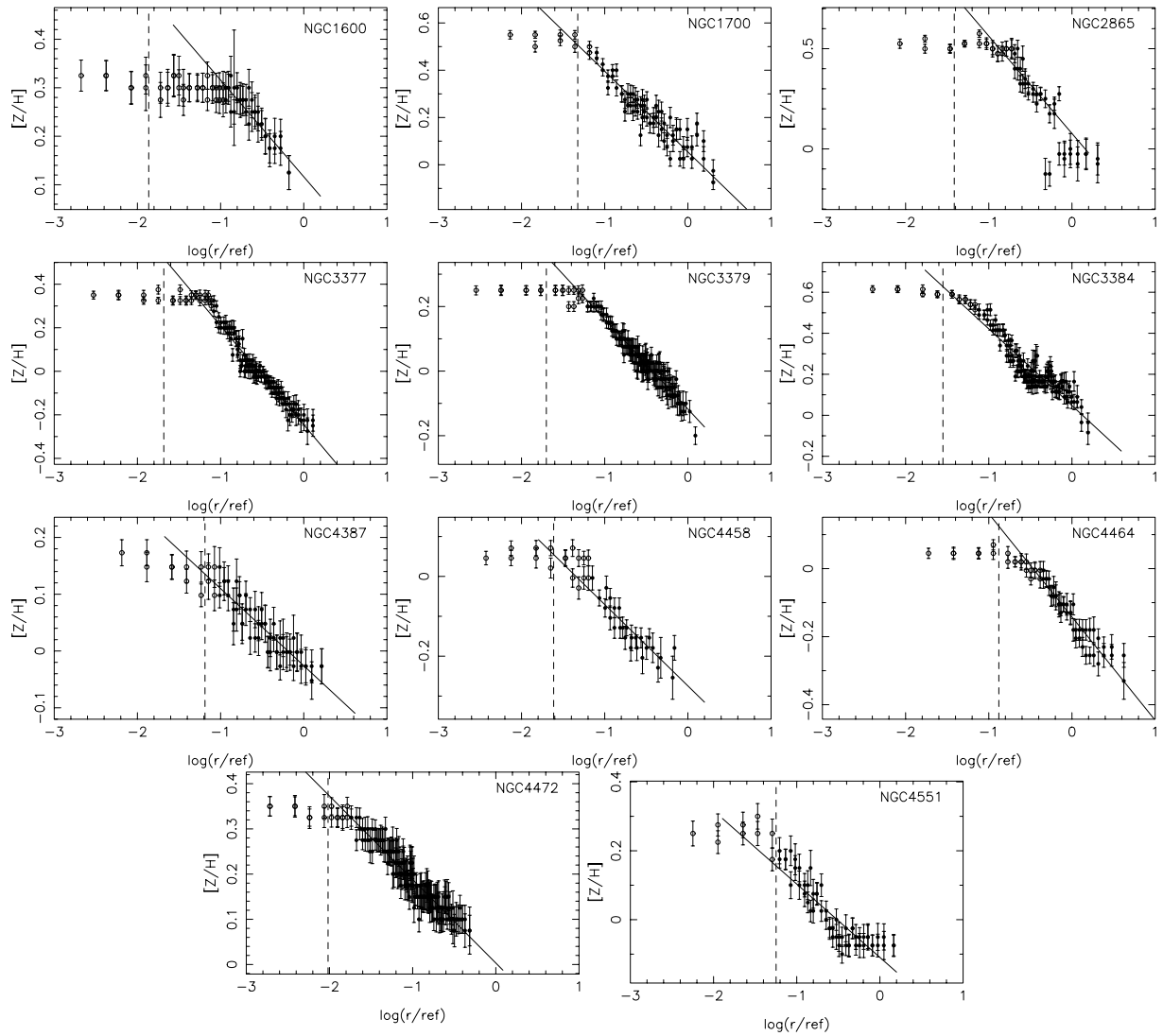

Figure 5. SSP-equivalent-[Z/H] profiles for the galaxies of the sample calculated with TMB03 models using a set of 19 different line-strength indices (see text for details). Solid lines represent a linear fit to the data weighting with the errors in the *y* direction. Only solid points have been fitted. Dashed lines indicate the extent of the seeing disc.

The only way to deal with this is to use a deconstruction method to analyse the whole star formation history of the galaxy (e.g. Panter, Heavens & Jimenez 2003; Ocvirk et al. 2006a,b). This will be done in a future paper. Instead, in the present work, we check the robustness of our results by comparing our gradients with the ones obtained using different indices and models. In particular, we will compare the age, metallicity and [E/Fe] gradients obtained as described above with the ones obtained as follow: (1) using a set of three indices: Fe4383, Hβ and Mgb; (2) using 19 indices, but clipping the indices that deviate more than 3σ from the fit; (3) using the models by Vazdekis et al. (2007)[2] and a the indices Fe4383, Hβ and Mgb. The last option is being shown as an extreme case of a completely different technique and model and serves a purpose in showing the robustness of the results against the technique and models employed.

(1) We selected Hβ, Fe4383 and Mgb because the models do an excellent job fitting these indices to globular clusters measurements and also because they have the highest sensitivities to the parameters we want to measure, i.e. age, Fe and Mg abundances, respectively. We perform a linear fit to the final values with radius in the same way as described above. The gradients are shown in Table 3.

(2) Although we decided to use the same indices for all the galaxies and along the radius to avoid any possible bias in the result due to the different sensitivity of the different indices to different chemical compositions, here we compare with the results obtained when a 3σ clipping is applied during the χ^2 minimization as in the original method described by Proctor & Sansom (2002).

(3) Finally, we also calculate the stellar population parameters along the radius using the new stellar population models by Vazdekis et al. (2007). These models are built for solar chemical composition and they are only calibrated for variations of age and [Z/H]. To derive [E/Fe] values, we followed the same procedure as in Trager et al. (2000a, hereafter T00a), with the only difference that we use the new fitting functions of Korn et al. (2005) instead of the Tripicco & Bell (1995) ones used by T00a. We include in the enhanced group ([X/H] = +0.3) the elements C, N, O, Mg, Fe, Ca, Na, Si, Cr and Ti, while the elements Cr, Mn, Co, Ni, Cu and Zn are depressed

[2] Available at http://www.ucm.es/info/Astrof/users/pat/models.html

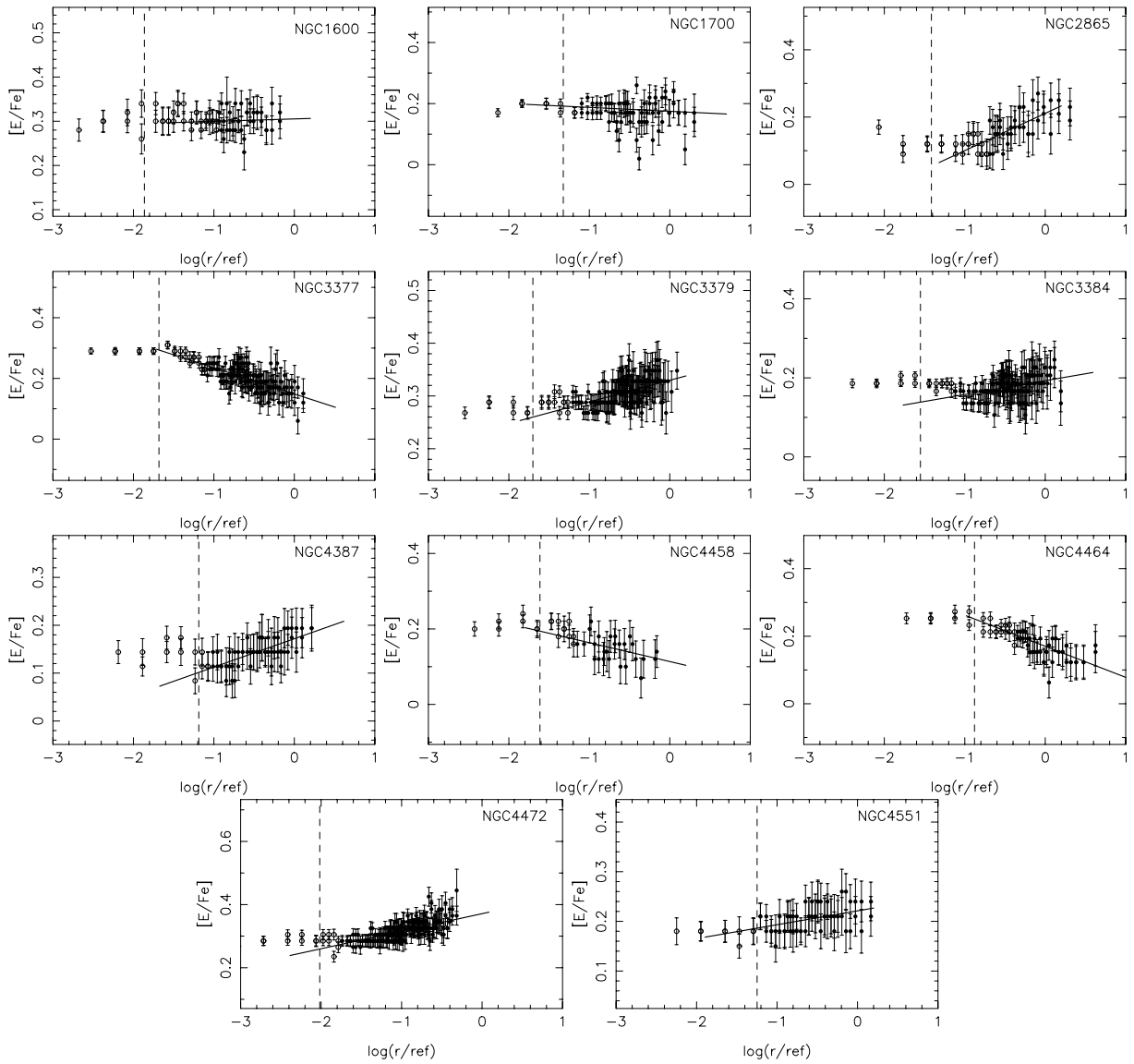

Figure 6. SSP-equivalent-[E/Fe] profiles for the galaxies in the sample calculated with TMB03 models using a set of 19 different indices. The solid lines represent linear fits to the solid points weighting with the errors in the y direction. The open symbols are those excluded from the fit. Dashed lines indicate the extent of the seeing disc.

by [X/H] $= -0.3$. We interpolate the model grid at intervals of 0.1 Gyr in age and 0.05 in metallicity. Then we applied the response functions by Korn et al. (2005) to obtain an interval step of 0.05 in [E/Fe]. Stellar population equivalent parameters were derived by choosing the best-fitting age, [Z/H] and [E/Fe] for the indices Hβ, Fe4383 and Mgb.

Fig. 7 represents the comparison of the gradients calculated with all the 19 indices as described at the beginning of the section with the methods (1), (2) and (3) described above. Table 4 shows the mean offset and residual dispersion of the comparison, calculated as the quadratic difference between the measured dispersion and the one expected from the errors.

As can be seen, significant offsets do not exist between the gradients calculated with a different number of indices. We do not even find significant offsets between the gradients calculated with different models and different number of indices. The rms dispersion in the comparison of the methods with and without clipping is compatible with the errors, however, the dispersion among the 1:1 relation in the comparison of the methods (1) and (3) with the method employing 19 indices is larger than the one expected by the errors. This should prevent us drawing conclusions that are not confirmed using the gradients measured with all the different methods.

In the rest of the paper we use the gradients derived with 19 indices without clipping because the errors on the parameters are smaller. We have checked, though, that none of the conclusions would change if we used the ones calculated with any of the other methods described above.

6 CENTRAL VALUES

In order to compare the gradients with the central values, we also extracted, for each galaxy, a spectrum within an aperture of 1.5 arcsec $\times\, r_{\rm eff}/8$ and used the corresponding line-strength indices to derive stellar population parameters. Fig. 8 shows the classical relations

Table 3. Age, [Z/H] and [E/Fe] gradients for the 11 galaxies in our sample calculated with a χ^2 minimization with different number of indices and different models. See text for details.

Galaxy	Grad age		Grad [Z/H]		Grad [E/Fe]	
	(19 indices) (TMB03)	(3 indices) (TMB03)	(19 indices) (TMB03)	(3 indices) (TMB03)	(19 indices) (TMB03)	(3 indices) (TMB03)
NGC 1600	0.000 ± 0.000	0.000 ± 0.000	-0.193 ± 0.024	-0.269 ± 0.051	0.014 ± 0.047	0.011 ± 0.022
NGC 1700	0.117 ± 0.052	0.035 ± 0.057	-0.342 ± 0.011	-0.229 ± 0.074	-0.014 ± 0.010	-0.070 ± 0.056
NGC 2865	1.153 ± 0.046	1.737 ± 0.129	-0.514 ± 0.018	-0.752 ± 0.088	0.094 ± 0.018	0.178 ± 0.064
NGC 3377[a]	0.237 ± 0.050	0.034 ± 0.018	-0.466 ± 0.009	-0.316 ± 0.036	-0.082 ± 0.009	-0.043 ± 0.040
NGC 3379	0.000 ± 0.000	0.000 ± 0.000	-0.278 ± 0.006	-0.238 ± 0.033	0.041 ± 0.006	0.015 ± 0.025
NGC 3384	0.086 ± 0.040	0.086 ± 0.040	-0.381 ± 0.008	-0.374 ± 0.051	0.028 ± 0.007	0.035 ± 0.023
NGC 4387	0.000 ± 0.000	0.000 ± 0.000	-0.135 ± 0.011	-0.117 ± 0.040	0.058 ± 0.014	0.064 ± 0.048
NGC 4458	0.000 ± 0.000	0.000 ± 0.000	-0.239 ± 0.020	-0.207 ± 0.035	-0.051 ± 0.025	0.140 ± 0.056
NGC 4464	0.000 ± 0.000	0.000 ± 0.000	-0.306 ± 0.017	-0.229 ± 0.036	-0.091 ± 0.021	-0.040 ± 0.042
NGC 4472	0.000 ± 0.000	0.000 ± 0.000	-0.186 ± 0.006	-0.155 ± 0.040	0.059 ± 0.005	0.054 ± 0.034
NGC 4551	0.028 ± 0.027	0.021 ± 0.023	-0.326 ± 0.023	-0.231 ± 0.072	0.033 ± 0.010	0.031 ± 0.038
	(19 indices) with clipping	(3 indices) V07 models	(19 indices) with clipping	(3 indices) V07 models	(19 indices) with clipping	(3 indices) V07 models
NGC 1600	0.052 ± 0.037	0.096 ± 0.123	-0.206 ± 0.065	-0.127 ± 0.113	0.026 ± 0.032	-0.049 ± 0.047
NGC 1700	0.124 ± 0.068	0.078 ± 0.133	-0.346 ± 0.057	-0.166 ± 0.106	0.002 ± 0.052	-0.087 ± 0.079
NGC 2865	1.043 ± 0.182	0.713 ± 0.086	-0.645 ± 0.216	-0.642 ± 0.107	0.025 ± 0.139	-0.161 ± 0.066
NGC 3377	0.363 ± 0.092	0.319 ± 0.152	-0.609 ± 0.080	-0.532 ± 0.099	-0.163 ± 0.051	-0.163 ± 0.052
NGC 3379	-0.011 ± 0.032	0.047 ± 0.105	-0.294 ± 0.038	-0.258 ± 0.084	0.020 ± 0.020	-0.020 ± 0.036
NGC 3384	0.083 ± 0.053	0.195 ± 0.113	-0.406 ± 0.057	-0.427 ± 0.125	0.015 ± 0.025	-0.016 ± 0.044
NGC 4387	0.002 ± 0.009	0.028 ± 0.120	-0.140 ± 0.041	-0.162 ± 0.032	0.064 ± 0.051	0.035 ± 0.048
NGC 4458	0.004 ± 0.008	0.105 ± 0.124	-0.138 ± 0.043	-0.363 ± 0.106	0.092 ± 0.075	-0.017 ± 0.062
NGC 4464	0.000 ± 0.000	0.197 ± 0.125	-0.348 ± 0.038	-0.396 ± 0.103	-0.116 ± 0.029	-0.194 ± 0.068
NGC 4472	0.000 ± 0.000	0.137 ± 0.122	-0.181 ± 0.032	-0.267 ± 0.100	0.046 ± 0.021	0.045 ± 0.047
NGC 4551	0.155 ± 0.079	0.058 ± 0.113	-0.354 ± 0.101	-0.189 ± 0.080	-0.021 ± 0.051	0.020 ± 0.045

[a]The age profile in this galaxy is not linear.

between the Mgb and the central velocity dispersion for our sample of galaxies. Table D1, in Appendix D, shows all the central indices and the central velocity dispersion. The values of the mean SSP-age, -metallicity and -[E/Fe] as derived with 19 indices are reported in Table 5.

Fig. 9 shows the relation of the age, metallicity and [E/Fe] with the central velocity dispersion. We have separated the galaxies – with different symbols – as a function of their central ages. As can be seen, contrary to what happens when the indices are compared with this parameter, the relations appear to have considerable dispersion. We analyse separately the three relations.

[Z/H] versus σ: the relations between the Mg_2 index and σ and the colour–magnitude relations have been interpreted, classically, as a mass–metallicity relation for early-type galaxies (e.g. Kodama & Arimoto 1997), in the sense that more massive galaxies are also more metal rich. However, it is clear from Fig. 9 that we do not detect a correlation between the metallicity and the velocity dispersion. Old galaxies (with ages >8 Gyr) define a mass–metallicity sequence, but galaxies with intermediate- or young ages, lie above the relation in such a way that the deviation from the relation correlates with the light-weighted mean age. The same result was obtained by Jørgensen (1999) and Trager et al. (2000b). Trager et al. (2000b) showed that galaxies are in a plane within the space of age, [Z/H] and σ, where, at a given σ, galaxies more metal rich are also younger. In the figure we have plotted the best linear relation found by Nelan et al. (2005) and the rms dispersion found by those authors. As can be seen, the oldest galaxies of our sample (with ages >8 Gyr) follow a very similar relation than the one found by these authors, but the younger galaxies deviate systematically from the relation. As several authors have noted before the fact that, at a given σ, younger galaxies are also more metal rich and have very important implications as, if real, the tightness of the colour–magnitude relation should not be interpreted as a low dispersion in the mean stellar ages of galaxies. This is because the effect that a rejuvenation of the stellar population has in the line-strength indices and colour is very similar to a decrease in metallicity – the so-called age–metallicity degeneracy (see e.g. Worthey 1994). This should be taken into account, also, when interpreting the evolution of the colour–magnitude diagram with redshift.

The result shown here and in the studies mentioned above challenges the interpretation of the colour–magnitude relation as a purely mass–metallicity relation, as usually assumed in the literature, as galaxies with the same mass can show a large spread in their metallicities.

[E/Fe] versus σ: several authors have found the existence of a positive correlation between the degree of α enhancement in the central parts of early-type galaxies and σ (Faber, Worthey & González 1992; Worthey, Faber & González 1992; Jørgensen 1999; Kuntschner 2000; Trager et al. 2000b; Terlevich & Forbes 2002; Nelan et al. 2005; Thomas et al. 2005). α elements and Fe-peak elements are released into the interstellar medium by different stars and on different time-scales. Therefore, it is common in the literature to use [E/Fe] as a cosmic clock to quantify the duration of the star formation. The reported relation between the ratio [E/Fe] and σ would imply, in this context, that more massive galaxies formed their stars in shorter time-scales. The relation between the [E/Fe] and the central velocity dispersion is, however, not very clear in our data (a non-parametric Spearman rank order test gives a probability of no

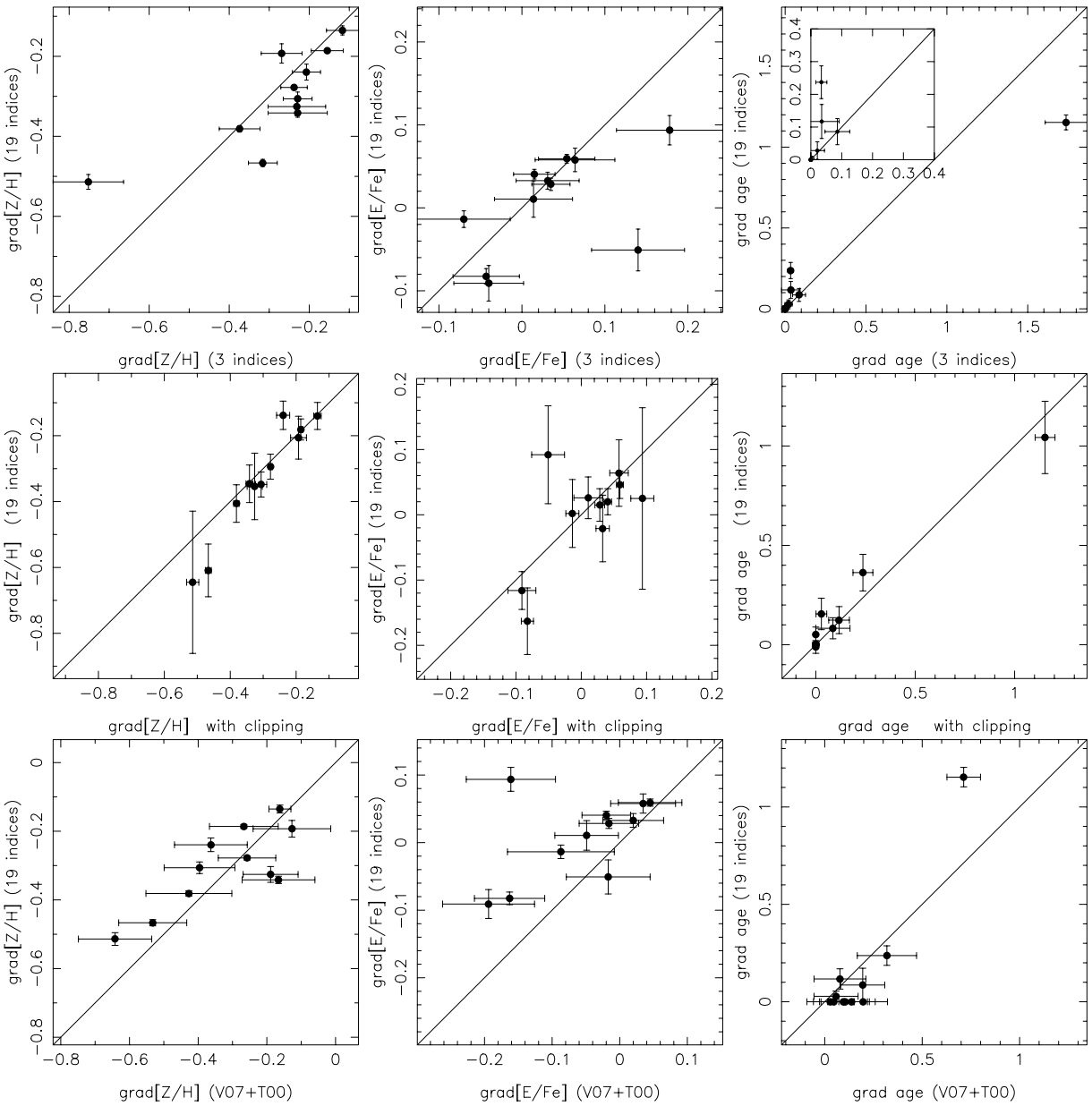

Figure 7. Comparison between the gradients of SSP-equivalent parameters calculated with the TMB03 models using all 19 indices and the ones obtained with the following methods: (1) using TMB03 models and only the indices Fe4383, Hβ and Mgb (upper panels); (2) using TMB03 models and 1ll 9 indices, but clipping the indices deviating more than 3σ from the best fitting (mid panels); (3) using Vazdekis et al. (2007) models (combined with the T00a method to derive [E/Fe]) and the indices Fe4383, Hβ and Mgb (lower panels).

correlation of ∼5 per cent, which is less than 2σ significance). The most massive galaxies are the ones with higher [E/Fe], but there is considerable scatter at lower σ. We have also plotted, in the figure, the relation found by Nelan et al. (2005) using ∼500 galaxies. As can be seen our galaxies follow the same relation, and the lack of correlation may be due to the small sample size.

Finally, we present in the bottom panel of Fig. 9 the relation between the central age and the central velocity dispersion. Contrary to what has been reported in many studies (e.g. Caldwell et al. 2003; Nelan et al. 2005; Bernardi et al. 2006; Sánchez-Blázquez et al. 2006c) we do not find any relation between these two parameters. Although we do not find young galaxies with $\sigma > 200\,\mathrm{km\,s^{-1}}$, we find a very large dispersion in the ages of galaxies with $\sigma < 200\,\mathrm{km\,s^{-1}}$. In the figure we also show the relation found by Nelan et al. (2005). It can be seen that the youngest galaxies in our sample clearly deviate from the relation found by those authors, although the rest of the galaxies are consistent with it.

7 GRADIENTS OF AGE, [FE/H] AND [E/FE]

The variation of the physical properties of galaxies with radius proves invaluable information for constraining the processes of galaxy formation and evolution. In the following sections we will analyse the relation between the stellar population parameters and other properties of the galaxies trying to understand the mechanism dominating the formation of the measured gradients.

Table 4. Comparison of the SSP-equivalent-parameter gradients derived using different methods: mean offset, rms dispersion, rms dispersion expected by errors and rms residual (not explained by the errors) in the comparison of the gradients measured with a χ^2 minimization and 19 indices without clipping and the following methods: (1) TMB03 (3 indices): using TMB03 models and only the indices Fe4383, Hβ and Mgb; (2) TMB03 (19 indices, clipping): using TMB03 models and a χ^2 minimization technique, clipping the indices that deviate more than 3σ from the final fit; (3) V07 models (3 indices): using Vazdekis et al. (2007) models and only the indices Hβ, Fe4383 and Mgb indices.

	TMB03 models 3 indices				TMB03 models 19 indices (clipping)				V07 models 3 indices			
	Offset	rms	rms (exp)	rms (res)	Offset	rms	rms (exp)	rms (res)	Offset	rms	rms (exp)	rms (res)
Grad age	0.002	0.03	0.02	0.022	0.000	0.000	0.000	0.000	0.007	0.197	0.122	0.155
Grad [Z/H]	−0.043	0.07	0.05	0.048	−0.006	0.049	0.051	0.000	−0.014	0.080	0.077	0.022
Grad [E/Fe]	−0.009	0.05	0.04	0.030	−0.014	0.030	0.035	0.000	−0.053	0.059	0.052	0.028

Table 5. Central values (within an aperture of 1.5 arcsec $\times$ $r_{\rm eff}/8$) for the age, [Z/H] and [E/Fe] measured in our sample of galaxies.

Galaxy	Age (Gyr)	[Z/H]	[E/Fe]
NGC 1600	13.5 ± 0.1	0.326 ± 0.003	0.357 ± 0.004
NGC 1700	2.9 ± 0.03	0.627 ± 0.006	0.186 ± 0.002
NGC 2865	1.0 ± 0.01	0.523 ± 0.005	0.133 ± 0.001
NGC 3377	5.5 ± 0.05	0.343 ± 0.003	0.277 ± 0.003
NGC 3379	14.2 ± 0.1	0.244 ± 0.002	0.288 ± 0.003
NGC 3384	3.06 ± 0.03	0.591 ± 0.006	0.186 ± 0.002
NGC 4387	8.88 ± 0.09	0.123 ± 0.001	0.154 ± 0.001
NGC 4458	11.7 ± 0.1	0.021 ± 0.001	0.241 ± 0.002
NGC 4464	13.5 ± 0.1	0.067 ± 0.001	0.256 ± 0.003
NGC 4472	11.3 ± 0.1	0.352 ± 0.003	0.285 ± 0.003
NGC 4551	6.47 ± 0.06	0.247 ± 0.002	0.183 ± 0.002

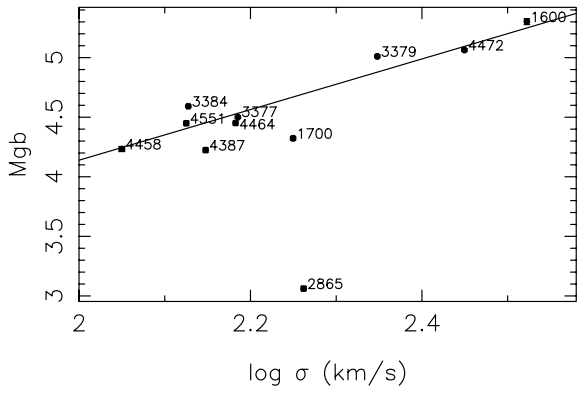

Figure 8. Relation between the Mgb index, measured in a aperture of 1.5 arcsec $\times$ $r_{\rm eff}/8$ versus the central velocity dispersion inside the same aperture.

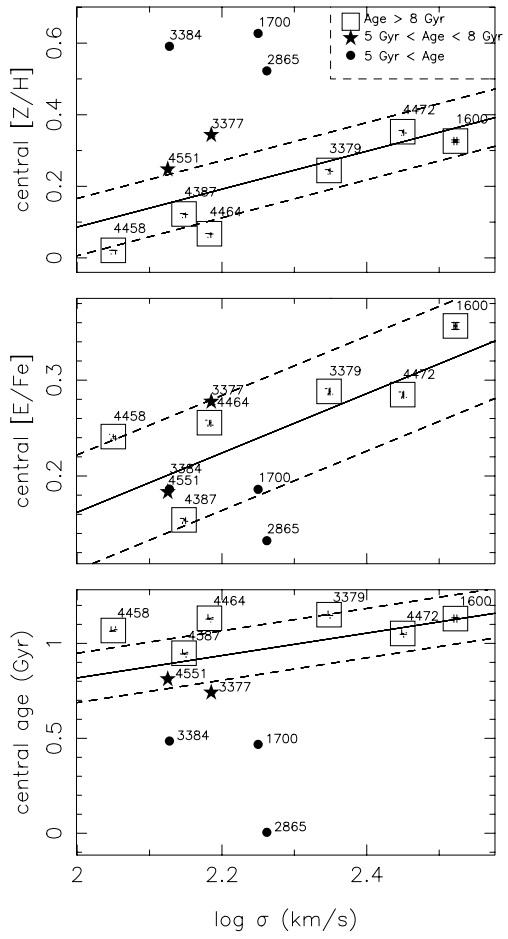

Figure 9. Relation between the central metallicity, α enhancement and age with the central velocity dispersion. Different symbols in the two panels indicate different central ages as indicated in the inset. Solid and dashed lines indicate the best linear fitting obtained by Nelan et al. (2005) and the 1σ errors obtained by those authors, respectively.

7.1 Age gradients

We find that for 10 of the 11 galaxies, age gradients are compatible with zero-slope. NGC 1700 shows a significant age gradient when this is measured using 19 indices, but this is not true if only three indices are employed, independently of the model used. NGC 3377 seems to show an age gradient, but the age profile in this galaxy does not behave as a power law, and, therefore, it does not make much sense to perform a linear fit. Several authors have analysed age gradients in samples of early-type galaxies but the results are still not conclusive. For example, Hinkley & Im (2001), Mehlert et al. (2003) and Wu et al. (2005) did not find any overall age gradient in their samples. Some other authors (e.g. González 1993; Silva & Elston 1994; Tantalo, Chiosi & Bressan 1998; Sánchez-Blázquez, Gorgas & Cardiel 2006d), however, have detected non-zero age gradients in their respective samples. The typical values found by those authors are ∼20 per cent variation, with the central parts younger than the external parts.

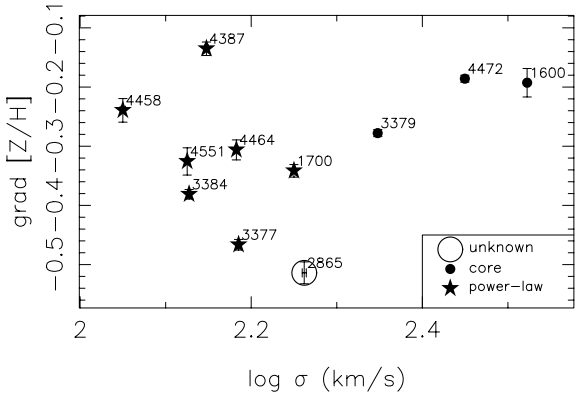

Figure 10. Relation between the metallicity gradient and the central velocity dispersion. Different symbols indicate different shapes of the inner profile as indicated in the inset.

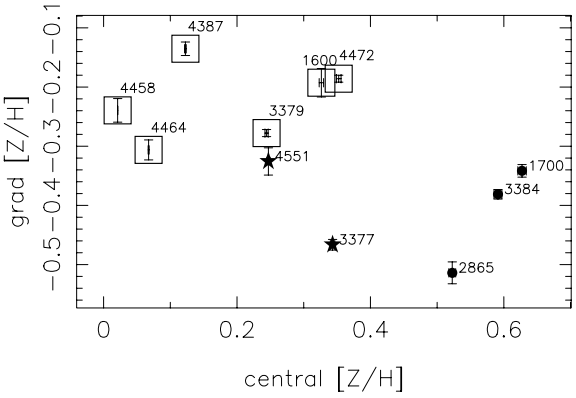

Figure 11. Relation between the metallicity gradient and the central metallicity. Different symbols show galaxies younger than 5 Gyr (filled circles), between 5 and 8 Gyr (stars) and older than 8 Gyr (squares).

7.2 Metallicity gradients

The mean [Z/H] gradient of our sample is Δ[Z/H]/log $r = -0.306$ with an rms dispersion of 0.133. This value suggests a mean reduction of metallicity in elliptical galaxies of more than 50 per cent per decade of variation in radius. This value is compatible with the values derived by other studies, e.g. Δ[Z/H]/log $r = -0.23 \pm 0.09$ (Gorgas et al. 1990); Δ[Z/H]/log $r = -0.25 \pm 0.1$ (Fisher, Franx & Illingworth 1995). In principle, the strength of the metallicity gradient is related to the merging history of the galaxies, as, while dissipational processes tend to create stronger gradients, mergers between galaxies destroy these gradients (e.g. Mihos & Hernquist 1994; Kobayashi 2004). The mean metallicity gradients for non-merger and merger galaxies derived by Kobayashi (2004) are Δ[Z/H]/Δlog $r \sim -0.30$ and -0.22, respectively. As can be seen, galaxies in our sample are compatible with both of these values. The direct comparison between the metallicity gradient obtained with single stellar population models and numerical simulations is, however, difficult, due to the manner by which the results from numerical simulations are transformed to the observational plane. Another way to determine the evolutionary paths of early-type galaxies is to study the relation between the metallicity gradients and other global properties of these systems, as different physical processes are expected to lead to different correlations. For example, dissipational processes are believed to create steeper gradients in more massive galaxies (Carlberg 1984; Bekki & Shioya 1999), although this is sensitive to the adopted feedback prescription in the simulations (e.g. Bekki & Shioya 1998, 1999). Dissipationless mergers of galaxies, on the contrary, are expected to produce some dilution of the gradients in galaxies (White 1980) deleting or producing an inverse correlation among stellar population gradients and luminosity.

Fig. 10 shows the correlation of the metallicity gradient with the velocity dispersion for our sample of galaxies. Although the sample is not very large, we confirm the lack of correlation previously noted by other authors using line-strength indices (e.g. Gorgas et al. 1990; Davidge 1991, 1992; Davies et al. 1993; Mehlert et al. 2003). Galaxies with steeper gradients are not the most massive of our sample but the ones with $\sigma \sim 200\,\mathrm{km\,s^{-1}}$.

A similar trend was found by Kormendy & Djorgovski (1989) between the colour gradients and M_B in a sample obtained by combining data with different quality from Vader et al. (1988), Franx, Illingworth & Heckman (1989) and Peletier, Lauberts & Valentijn (1989). Carollo et al. (1993) compared the Lick index Mg_2 gradient and both the mass and the luminosity (derived from the Fundamental Plane), and they concluded that there is a change in the slope of the trends approximately at the same mass as found here. They also found a significant correlation between the gradients and mass for galaxies with $M_{\rm tot} \leqslant 10^{11}\,\mathrm{M}_{\odot}$, where $M_{\rm tot}$ represents the total mass of the galaxy. Our sample is too small to perform reliable statistical tests to study the significance of the correlations in the two magnitude ranges. Confirming the presence of a slope change in the grad [Z/H]–σ plane at $M_B \sim -21.5$ will require a larger sample of comparable quality to that presented here. However, there is a significant degree of evidence now which indicates that the metallicity gradient is not constant with the mass of the galaxies, but gets steeper for galaxies around this magnitude.

As we said earlier, the correlation between the metallicity gradient and the mass of the galaxies in the context of mergers of galaxies depends on the degree of dissipation in the merging. A positive correlation, as suggested by some authors (e.g. Carollo et al. 1993; this study) for galaxies with $M_B > -20.5$, is expected in mergers with gas (Bekki & Shioya 1999), while the opposite trend (as suggested by some studies e.g. Franx 1988; Vader et al. 1988) is expected in dissipationless mergers, assuming that more massive galaxies have suffered more mergers (as predicted by hierarchical models of galaxy formation). Therefore, if the trends are confirmed, they could be explained assuming a decrease, with the mass of the galaxy, of the degree of dissipation during the last major merger event.

Several studies (Carollo, Dazinger & Buson 1993; González & Gorgas 1995) have found that galaxies with stronger central Mg_2 indices showed, also, steeper Mg_2 gradients. Although other authors (Kobayashi & Arimoto 1999; Mehlert et al. 2003) have failed to find this correlation, it has been recently confirmed by some studies (Kuntschner et al. 2006; Sánchez-Blázquez et al. 2006d). However, Kuntschner et al. (2006) claim that the correlation is driven by S0 galaxies or, in particular, by young galaxies. If the central metallicity values were correlated with the metallicity gradient, it would imply that the global metallicities of ellipticals were more similar than the central ones. Unless such aperture effects are taken into account, the impact upon the interpretation of scaling relations – such as the redshift evolution of the colour–magnitude relation – could be significant.

In Fig. 11 we have plotted this relation, but using the metallicity instead of the Mg_2 index. We have separated, with different symbols, galaxies in different ranges of central ages. There exists a trend for which galaxies with higher central metallicities also show

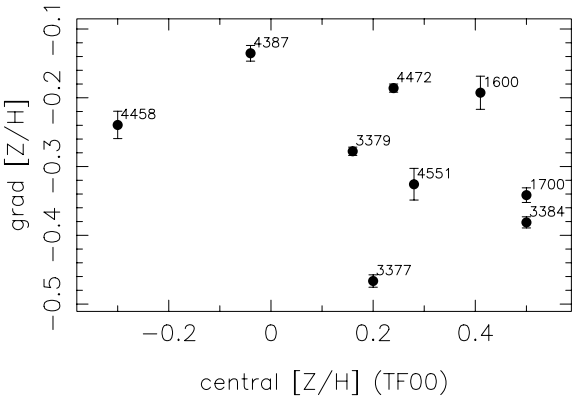

Figure 12. Correlation between the metallicity gradient measured in this work and the independent central metallicity values extracted from Terlevich & Forbes (2000).

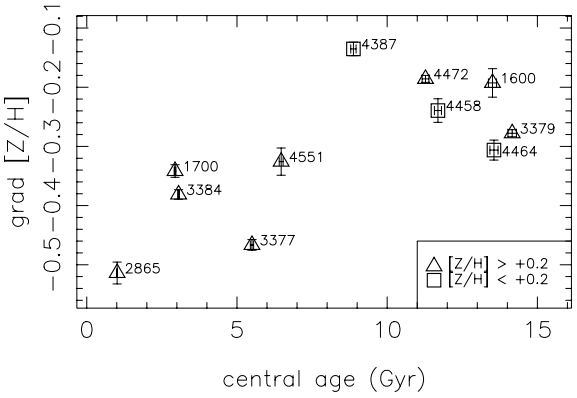

Figure 13. Relation between the metallicity gradient and the central age. Different symbols represent galaxies with metallicity higher (triangles) and lower (squares) than [Z/H] $= +0.2$ as indicated in the inset.

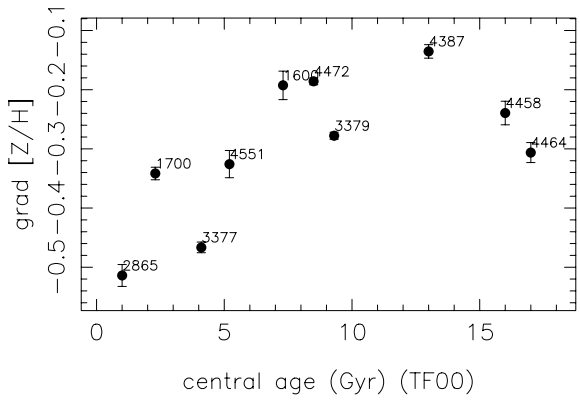

Figure 14. Relation between the metallicity gradient calculated in this study and the independent central mean age of the galaxies extracted from Terlevich & Forbes (2000).

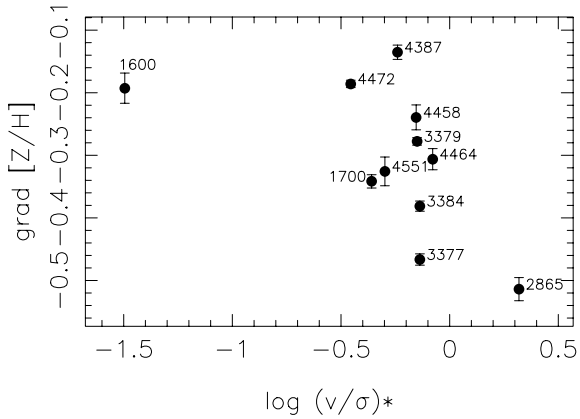

Figure 15. Relation between the metallicity gradient and the anisotropy parameter normalized to an oblate rotator (Bender 1990).

steeper gradients in this parameter, although there is considerable scatter among the relation. A non-parametric Spearman rank-order test gives a level of significance lower than 0.05 (or a probability of correlation of 95 per cent), which is the limit to claim a correlation. In principle, this correlation could be the consequence of the correlation of the errors, as an increase in metallicity in the centres would produce also an increase in the metallicity gradient. To check this possibility we have represented, in Fig. 12, the relation between our metallicity gradients and the central ages from other authors. In particular, we have used the values obtained by Terlevich & Forbes (2002) using Worthey (1994) stellar population models and the combination of indices Mgb, ⟨Fe⟩ and Hβ collected by different studies. As can be seen, the trend is still present even using completely independent values, which argues against the correlation of the errors being the only reason for its existence.

To explore the relation between the metallicity gradient and the central age of the galaxies we have represented, in Fig. 13, these two magnitudes. Furthermore, as can be seen, the correlation is obvious for galaxies with central ages less than 10 Gyr. For the whole sample, a rank-order Spearman correlation test gives now a probability of non-correlation lower than 1 per cent. We have also separated the galaxies with central metallicities higher (stars) and lower (circles) than [Z/H] $= +0.2$. In general, galaxies showing steeper metallicity gradients are more metal rich and younger while galaxies with shallower metallicity gradients are older. For galaxies older than 10 Gyr, however, half of the sample have low metallicities in their centre, while half of the sample show metallicities higher than [Z/H] $= +0.2$ (see Table 5). The galaxies with larger metallicity are the most massive galaxies of our sample, with $\sigma > 200\,\mathrm{km\,s^{-1}}$. The correlation between the metallicity gradient and the central age has been previously found by Sánchez-Blázquez et al. (2006d) (although the methodology is very different to this work and the correlation is only found when the metallicity is measured with some indicators). As we did before, we checked the possibility that the correlation was artificial, due to the correlation of the errors. To do that we plotted the metallicity gradients against the completely independent ages extracted from the Terlevich & Forbes (2000) catalogue. This can be seen in Fig. 14. It is clear, as before, that the correlation is not an exclusive consequence of the correlation of the errors.

Finally, we study the relation between the metallicity gradient and the rotation of the galaxies and the shape of their isophotes. The decreasing rotational support and transition from discy to boxy isophotal shapes with increasing stellar mass in elliptical galaxies suggests an increasing fraction of dissipationless mergers in the growth of the most massive elliptical galaxies (e.g. Bender, Burstein & Faber 1992; Kormendy & Bender 1996; Faber et al. 1997; Naab, Khochfar & Burkert 2006b). Fig. 15 shows the relation between the metallicity gradient and the anisotropy parameter ($\log(v/\sigma)$*) as defined in Bender (1990) normalized by the value expected for an isotropic oblate galaxy flattened by rotation. To derive this parameter we followed the procedure described in Pedraz et al. (2002).

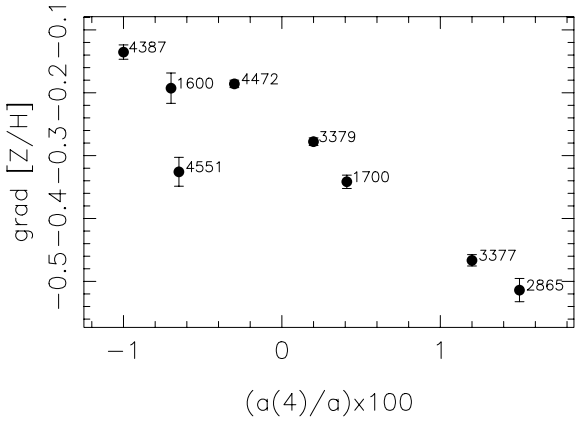

Figure 16. Relation between the metallicity gradient and the parameter (a4/a) × 100, extracted from Bender et al. (1989).

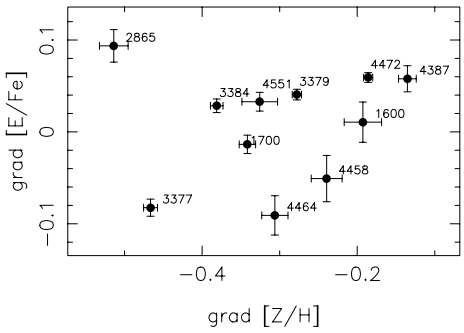

Figure 17. Relation between the [E/Fe] gradient and the metallicity gradient for our sample of galaxies.

A conservative estimate of the maximum rotation velocity (v) was computed as the error-weighted mean of the two data pairs with the highest rotational velocities. To compute the mean velocity dispersion we co-added all the individual spectra with radii between the seeing limit and the effective radius. Prior to this, we shifted all the spectra to rest frame using the rotation curves. The final values for the sample of galaxies presented here are listed in Table 1. A non-parametric Spearman rank-order test gives a significant correlation with a level of significance lower than 0.05. However, we are aware that this correlation is driven mainly by two galaxies (NGC 1600 and 2865) and that larger samples would be necessary to confirm its existence.

Fig. 16 shows the relation between the metallicity gradient and the parameter (a4/a) × 100, which measured the deviation of the shape of the isophotes from a perfect ellipse. Positive values of a4 indicate discy isophotes while a4 < 0 indicates that the isophotes have a boxy shape. Most of the values were taken from Bender et al. (1989), who defined this parameter as the peak value of a4/a in the case of peaked profiles and the value at 1 effective radius in the case of monotonically increasing or decreasing profiles. For the galaxy NGC 2865, the value was extracted from Reda et al. (2004). We could not find references (measured in the same way) for three of our galaxies: NGC 3384, 4458 and 4464 and, therefore, they are not included in the figure. For the rest of the galaxies, there exists a strong correlation between grad[Z/H] and (a4/a) × 100. Discy galaxies show stronger gradients and the strength of the gradient gets lower with the boxiness of the isophotes. This strong correlation is surprising as the a4 parameter measured in simulated galaxies depends on the projection effects, and therefore, the same galaxy can have boxy and discy isophotes depending of the viewing angle (Stiavelli, Londrillo & Messina 1991; Governato, Reduzzi & Rampazzo 1993; Heyl, Hernquist & Spergel 1994; Lima-Neto & Combes 1995; Gibson et al. 2007). Bekki & Shioya (1997) performed numerical simulations of mergers between gas-rich galaxies, studying the effect of star formation on the structural parameters of the remnant. They found that the rapidity of gas consumption by star formation greatly affects the isophotal shape of the merger remnant. Mergers with gradual star formation are more likely to form elliptical galaxies with discy isophotes, while those where the star formation is more rapid are more likely to form boxy ellipticals (although this depends on the viewing angle and, therefore, these scenario can lead to galaxies that can be seen as discy too). This scenario could explain the relation between the metallicity gradient and the shape of the isophotes found here. Furthermore, if the metallicity gradients are correlated with the shape of the isophotes and also with the central values of age and metallicity, this implies that the young ages observed in many early-type galaxies are not the consequence of a frosting population that form, for example, due to the accretion of small galaxies, but that the physical process that produced the recent star formation is related with the process shaping the gradients in the galaxies. This could happen, for example, in a scenario of mergers between galaxies.

7.3 Chemical abundances gradients

The chemical abundance ratios variations with radius give information about the time-scales of the star formation within the galaxies.[3] Fig. 6 shows the [E/Fe] gradients for our sample of galaxies. As can be seen in the figure, galaxies show a broad variety in the slope of the [E/Fe] profiles. In particular, contrary to what it would be expected by models of dissipative collapse, some of the galaxies show negative [E/Fe] gradients, indicating, *if* interpreted assuming a single episode of star formation, more extended star formation histories in the external parts.

Several theoretical works have studied the [Mg/Fe] gradients using chemical and cosmological chemodynamical evolution cores. Martinelli et al. (1998) and Pipino et al. (2006) modelled the scenario suggested by Franx & Illingworth (1990) where metallicity gradients are the consequence of the time delay in the development of galactic winds between the central and external parts of the galaxies. In this scenario stars in the outermost regions form earlier and faster than the ones in the centre and, therefore, a natural outcome from this model is an increase of the [Mg/Fe] ratio with radius. In particular, the recent work by Pipino et al. (2006) predicts a value of grad [E/Fe] $\sim +0.2$–0.3 dex, which reproduces the observations by Méndez et al. (2005) but it is steeper than any of the gradients measured here. In this scenario, the duration of the star formation is the only parameter controlling the local metallicity. Therefore, we would expect to find a correlation between the [Z/H] and the [E/Fe] gradients (under the assumption that [E/Fe] is a good measure of the time-scales of the star formation).[4] Fig. 17 shows the relation between both gradients. As can be seen, we do not detect any significant correlation in our sample of galaxies; a non-Spearman

[3] This is true if we assume that there is no variations of the initial mass function (IMF) along the radius and that the feedback processes blow away all the elements with the same efficiency.

[4] Other scenarios can produce differences in the [E/Fe] ratio, as differences in the IMF or selective loss of gas. See e.g. (Faber et al. 1992; Worthey 1998; Trager et al. 2000b) for details.

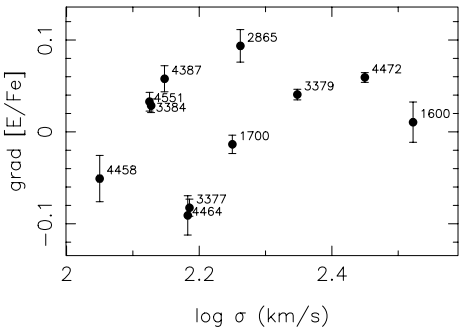

Figure 18. Relation between the [E/Fe] gradient and the central velocity dispersion of the galaxies.

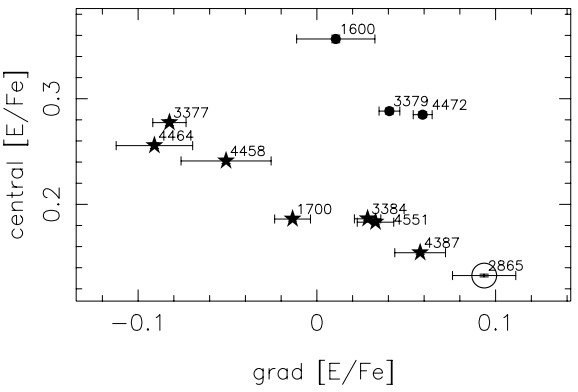

Figure 19. Central [E/Fe] inside a $r_{\rm eff}/8$ aperture as a function of the [E/Fe] gradient. Symbols are the same as in Fig. 10: stars and circles represent galaxies with *power-law* and *core* inner profiles, respectively.

rank order coefficient shows a probability of correlation lower than 40 per cent.

On the other hand, cosmological and semicosmological chemodynamical simulations by Gibson et al. (2007) and Kobayashi (2004), respectively, predict slightly shallower values, although still steeper than the values obtained here. In particular, Gibson et al. (2007) quoted, for a galaxy with $\sigma \sim 250\,{\rm km\,s^{-1}}$ a value of grad [E/Fe] $= +0.1$, while Kobayashi (2004) gives mean values of grad [E/Fe] $= +0.15$ and $+0.2$ for non-major mergers and major mergers galaxies, respectively.

There have been two previous studies presenting [E/Fe] gradients with high quality data in two individual galaxies. Méndez et al. (2005) found a positive gradient in the galaxy NGC 4697 which was reproduced by above quoted models of Pipino et al. (2006), and Proctor et al. (2005) analysed the gradient of the galaxy NGC 821, which showed a young population in its centre, finding a [E/Fe] gradient compatible with being zero or slightly negative. However, these authors claimed that if, as happens in the solar neighbourhood, oxygen does not track Mg in early-type galaxies, then the derived [E/Fe] could turn out to be positive.

Also Mehlert et al. (2003) derived [E/Fe] gradients for a sample of 35 early-type galaxies in the Coma cluster. They obtained a mean value of 0.05 ± 0.05 dex, and the deviation from the mean for all their objects can be explained by the errors alone. Therefore, they concluded that early-type galaxies show α/Fe gradients consistent with zero. This does not exclude, however, the presence of negative α/Fe gradients for some of the galaxies of their sample. In any case, the quality of this sample of gradients is not as high as the one in the other aforementioned studies. These authors also analysed the relation between the gradients of metallicity and [E/Fe] without finding any significant correlation.

In order to study whether galaxies with positive and negative [E/Fe] gradients are intrinsically different, we have analysed the relations between the slope of the gradient and other parameters of the galaxies. Fig. 18 shows the relation between the [E/Fe] gradients and the central velocity dispersion. A non-parametric rank-order Spearman test gives a non-significant correlation, although galaxies with negative gradients of [E/Fe] tend to be in the low mass end of our sample. We showed earlier in this section that there exists a correlation between the [Z/H] gradient and the central value of [Z/H]. In Fig. 19 we check the same relation for the values of [E/Fe]. With different symbols galaxies with *power-law* (stars) and *core* (circles) inner profiles are represented. This cut also corresponds to a cut in the central σ at $200\,{\rm km\,s^{-1}}$. As can be seen, there is a correlation between the central value of and the gradients in [E/Fe], but there seems to exist a dichotomy between galaxies with *core* (or galaxies with $\sigma > 200\,{\rm km\,s^{-1}}$ in our sample) and *power-law* (all galaxies with $\sigma < 200\,{\rm km\,s^{-1}}$ in our sample) inner profiles. For galaxies with a *power-law* inner profile we found a clear correlation between the central value and the gradient of the [E/Fe], while galaxies with a *core* profile lie above the relation. This different relation may be indicating fundamental differences in the formation processes of galaxies with σ lower and above $200\,{\rm km\,s^{-1}}$. This value could mark the transition between wet and dry mergers (Faber et al. 2005), and its physical motivation may be related to the thermal properties of inflowing gas in these galaxies and their interplay with feedback processes (Binney 2004; Dekel & Birnboim 2006). The transition between the cold flows and hot flows can be very sharp, especially if feedback from active galaxy nuclei is included.

When this mechanism is introduced in cosmological models of galaxy formation, most massive galaxies form their stars at high redshift and in very short time-scales and then have assembled later mainly through dry mergers (Cattaneo et al. 2006). This scenario can also explain the preferentially boxy isophotes of these systems, their lower rotation and their older stellar populations. If confirmed, it also supports the idea of biased merging, for which more massive galaxies merge, preferentially, with other massive galaxies, as predicted in the hierarchical models of galaxy formation (e.g. Kauffmann & Charlot 1998) and also supported in the relation of the metal-poor globular-cluster colours and the galaxy luminosity (Brodie & Strader 2006).

We explore now the correlation between the [E/Fe] gradient and the a4 parameter, which measures the degree of boxiness or disciness of the isophote shapes. As can be seen in Fig. 20, the correlation is not as clear as in the case of the [Z/H] gradient. If we exclude the galaxy NGC 2865 there is perhaps a trend for which galaxies with a more positive a4 show, also, a steeper, negative [E/Fe] gradient, but, clearly, NGC 2865 does not fit into this trend. This may represent a temporal state, as this galaxy shows a very young population in its centre (this galaxy also deviates from the Mgb–σ relation), but we cannot conclude anything without a larger sample.

Finally, we analyse the relation between the [E/Fe] gradient and the anisotropy parameter as we did in Section 7.2. Fig. 21 shows this relation. Contrary to that seen with the metallicity gradient, there is no significant correlation between these two parameters for the whole sample. However, if we eliminate the two most extreme galaxies (NGC 1600 and 2865) a non-parametric rank-order test gives a probability of no correlation lower than 1 per cent.

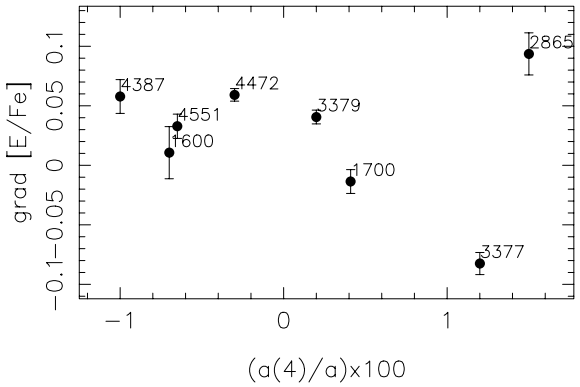

Figure 20. Relation between the [E/Fe] gradient and the parameter (a4/a) × 100, which indicates the deviation of the isophotes from perfect ellipses.

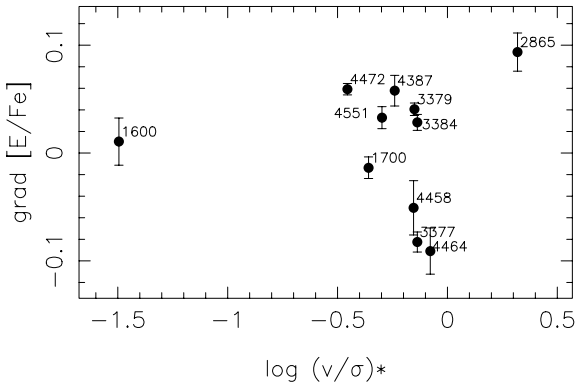

Figure 21. Relation between the [E/Fe] gradient and the anisotropy parameter for our sample of galaxies.

8 RELATION BETWEEN THE LOCAL STELLAR POPULATION PARAMETERS AND THE LOCAL VELOCITY DISPERSION

If galactic winds were the only mechanism responsible for the presence of metallicity gradients we might expect to find a correlation between the local metallicity and the local potential well, and between the metallicity and the [E/Fe] gradient. We showed in Section 7 that the latter is not present in our sample, but several authors have found correlations between the colours and metallicity gradients, and the local potential gradient, parametrized using either the escape velocity (Franx & Illingworth 1990; Davies et al. 1993) or the velocity dispersion (Mehlert et al. 2003). It is interesting to check if this correlation is present in our sample.

Fig. 22 shows the relation between [Z/H] at different galactocentric distances versus the velocity dispersion measured at the same location. To study the degree of correlation we performed a non-parametric Spearman-rank test. Table 6 shows the results of this test. Statistically significant correlations are marked with an asterisk. We have also drawn the result of an unweighted linear fit between the two parameters.

We do not find a strong correlation between the local metallicity and the local σ for *all* the galaxies in the sample. However, we do find correlations for seven out of 11 galaxies.

The correlation between the local metallicity and local σ arises naturally in a scenario where the star formation proceeds until the energy release by the supernova overcomes the binding energy and then the gas is expelled from the galaxy preventing more star formation. As pointed out by Franx & Illingworth (1990), dissipative models with inward flows of pre-enriched gas would, in principle, tend to destroy the correlation. However, Davies et al. (1993) also showed that due to anisotropy and rotation effects, the velocity dispersion is a poor indicator of the escape velocity, which could be also the reason for the lack of correlation in some of our galaxies.

9 DISCUSSION

Although almost all galaxies show radial abundance gradients, the origin remains a matter of debate. A radial variation of star formation rate (SFR), or the existence of radial gas flows, or a combination of these processes, can lead to abundance gradients in discs (e.g. Lacey & Fall 1985; Koeppen 1994; Edmunds & Greenhow 1995; Tsujimoto et al. 1995; Chiappini, Matteucci & Gratton 1997). Mergers are more complicated, because they depend on several parameters as the mass fractions of the systems merging, the amount of dissipation and possible associated star formation. However, under different scenarios we would expect differences in the strength of the gradients and in their relationship with other global galaxy parameters.

We have found, in the present paper, that early-type galaxies show null or very shallow age gradients, negative metallicity gradients, ranging from grad [Z/H] $= -0.19$ to -0.51 dex, and both, positive and negative, but very shallow, [E/Fe] gradients (from -0.09 to 0.06 dex). The existence of both positive and negative [E/Fe] gradients rule out simple outside-in scenarios where the gradient is an exclusive consequence of the delayed onset of the galactic winds in the central parts as suggested in some studies (e.g. Franx & Illingworth 1990; Martinelli et al. 1998; Pipino et al. 2006). This is also confirmed by the lack of correlation between [Z/H] and [E/Fe] gradients.

In the present paper, we have found a correlation between the metallicity gradient and both the shape of the isophotes, and the degree of rotational support. These trends are difficult to explain in monolithic scenarios of galaxy formation, but are well explained in scenarios of mergers where the degree of dissipation decreases with the mass. In this context, and assuming that the interaction triggers star formation in the centre of the remnant, the strength and the rapidity of the central burst (in general, the degree of dissipation during the interaction) would determine the shape of the isophotes (a4 becomes larger with the degree of dissipation, or with less efficient star formation), the central value of [E/Fe] (also higher for more efficient star formation) and the strength of the [Z/H] and [E/Fe] gradients – the later could become negative if the gas is transformed into stars very efficiently in very short time-scales (see Thomas et al. 1999).

The transition between mergers with gas and completely dissipationless mergers is believed to occur at a critical stellar mass of $3 \times 10^{10}\,\mathrm{M}_{\odot}$, which is the mass separating the red and blue sequence of galaxies (Kauffmann et al. 2003) in the colour–magnitude diagram. This mass corresponds roughly to the mass of the galaxies showing stronger gradients (Vader et al. 1988; Kormendy & Djorgovski 1989; this study). The dichotomy observed in the grad [E/Fe]–central [E/Fe] plane suggests that the transition is not gradual. In order to explain the existence of red and blue sequences in the colour–magnitude diagram of galaxies (Kauffmann et al. 2003), cosmological simulations also need to introduce a mechanism that sharply terminates the star formation in galaxies with stellar masses $M > 3 \times 10\,\mathrm{M}_{\odot}$. Feedback from active galactic nuclei (AGNs) is the most promising candidate for this extra source of heating

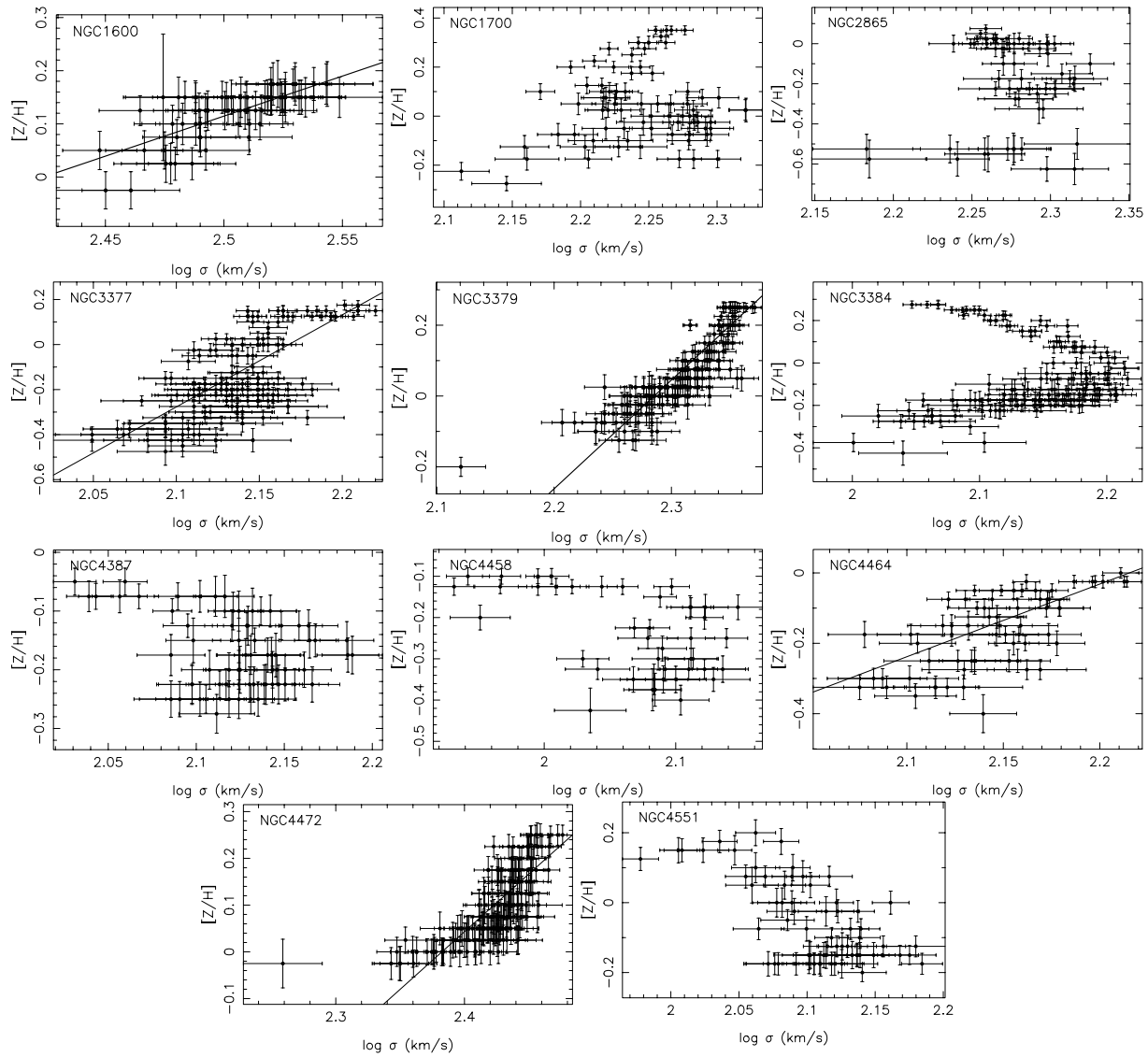

Figure 22. Relation between the local [Z/H] and the local velocity dispersion. Lines represent the best linear fitting to the data, when a significant correlation exists.

(Tabor & Binney 1993; Tucker & David 1997; Granato et al. 2004; Di Matteo, Springel & Hernquist 2005; Kawata & Gibson 2005).

We have also find, in the present study, a correlation between the metallicity gradient and both the central values of age (for galaxies younger than $\sim$10 Gyr) and metallicity. We have shown that these correlations are not entirely due to the correlation of the errors. If we assume, as suggested above, that abundance gradients are modified by the occurrence of major mergers, the fact that these gradients are correlated with the central values and with structural parameters as the shape of the isophotes, suggests that the young population found in the centre of some of our galaxies is the consequence of star formation triggered during major mergers.

This scenario, however, is not free from problems. Thomas et al. (1999) and Pipino & Matteucci (2006) have shown that is difficult to reach the high values of [Mg/Fe] in the centres of elliptical galaxies when massive secondary bursts of star formation are superimposed on an old population, *if* the new stars form from gas with abundances matching the ones of present day spiral galaxies, unless those stars form with an IMF flatter than that of the Salpeter (1955). These studies are potentially useful to constraint the amount of new stars that can be formed under this scenario. In a following paper, we will present this information and test the viability of this scenario from the chemical point of view.

The absence of age gradients in most of the galaxies also constraints the amount of new stars that can be formed in these episodes. However, due to the age–metallicity degeneracy, a burst of star formation older than 2 Gyr and more metal rich than the underlying population may produce very flat gradients in Hβ and stronger differences in the metallic indices. For example, the difference between two single stellar populations with ages 5 and 12 Gyr, metallicities [Z/H] $= -0.5$ and $+0.2$ and the same [E/Fe] would be -0.024 Å in Hβ, 1.2 Å in Mgb and 4.1 Å in C4668 which is compatible with the differences between the indices in the centre and at one effective radius for the galaxy NGC 3384, which shows a null age gradient.

The amount of gas present during the interaction to produce the observed trends and properties of the less massive galaxies does not need to be large. Numerical simulations of mergers of disc galaxies with a gas fraction for the progenitor galaxies of only 10 per cent

Table 6. Local metallicity and velocity dispersion correlation. t parameter and significance of the correlation between the local [Z/H] and the local velocity dispersion. A value of $\alpha < 0.01$ indicates that the probability that the correlation is by chance is lower than 1 per cent, which correspond to a 3σ correlation.

Galaxy	t	α
NGC 1600	5.3	2.5E−06*
NGC 1700	−0.18	0.429
NGC 2865	0.25	0.400
NGC 3377	6.26	2.9E−09*
NGC 3379	21.56	0.000*
NGC 3384	7.21	2.2E−11*
NGC 4387	2.00	0.025
NGC 4458	−0.11	0.456
NGC 4464	4.98	5.1E−06*
NGC 4472	14.84	1.9E−32*
NGC 4551	−2.64	0.005*

Notes. Statistically significant correlations are marked with an asterisk.

can reproduce the kinematical and photometric properties of intermediate-mass ellipticals (Jesseit et al. 2007). This is approximately the mass fraction of gas remaining in a galaxy at $z \sim 0.6$ before experiencing its last major merger in the cosmological simulations by Meza et al. (2003).

10 SUMMARY

We present measurements of stellar population parameter gradients with unprecedented quality for a sample of 11 early-type galaxies in the field and the Virgo cluster.

For most of the galaxies in our sample we find null or shallow age gradients, negative [Z/H] gradients ranging from −0.135 to −0.514 and *both*, negative and positive, although shallow, [E/Fe] gradients.

We do not find any strong correlation between the metallicity gradient and the central velocity dispersion of the galaxies. Galaxies with stronger metallicity gradients are those with $\sigma \sim 200\,\mathrm{km\,s^{-1}}$. For galaxies with σ below this limit there is a relation for which more massive galaxies show steeper metallicity gradients. This trend seems to change at $\sigma \sim 200\,\mathrm{km\,s^{-1}}$, as previously noted by other authors (e.g. Peletier et al. 1990; Vader et al. 1988), although we do not have enough galaxies with σ above this limit to confirm the result.

We found that metallicity gradient correlates with both central metallicity and central age, although the correlation with the central age is only visible for galaxies with mean ages below ∼10 Gyr. Galaxies with a younger central equivalent-SSP age show also steeper metallicity gradients and higher central metallicity.

Both [Z/H] and [E/Fe] gradients show strong correlations with the shape of the isophotes. The shape of the isophotes in a merger can be determined by the degree of dissipation during the interaction (e.g. Bekki & Shioya 1997). [Z/H] gradients do not correlate with [E/Fe] gradients, which challenges the scenario where the local potential well is the only responsible agent for the presence of gradients in early-type galaxies.

[E/Fe] gradients show a correlation with the central values of [E/Fe], but two different sequences are defined for galaxies with central σ less and greater than $200\,\mathrm{km\,s^{-1}}$. Most massive galaxies show a higher central [E/Fe] for a given [E/Fe] gradient than less massive ones.

In general, the presented gradients and their correlation with other parameters are compatible with a scenario where elliptical galaxies formed through the merger of smaller structures and the relative amount of dissipation experienced by the baryonic mass component along ellipticals stellar mass assembly decreases with increasing galaxy mass. However, two results, the trend between the metallicity gradients and the central σ and the relation between the gradient and central [E/Fe], suggest that this transition is not gradual but there is a sharp change in the properties of galaxies above and below $\sigma \sim 200\,\mathrm{km\,s^{-1}}$.

Although the quality of the gradients analysed here is very high, the sample is not very large. Therefore, the conclusions presented in this paper will need to be confirmed with larger samples.

ACKNOWLEDGMENTS

The authors wish to recognize and acknowledge the very significant cultural role and reverence that the summit of Mauna Kea has always had within the indigenous Hawaiian community. We are most fortunate to have the opportunity to conduct observations from this mountain. It is a pleasure to thank Harald Kuntschner for kindly provide us with the index gradients extracted from the SAURON data simulation the same angle for the position of the slit. PS-B thanks Cristina Chiappini, George Djorgovski and Daisuke Kawata for very fruitful discussions. Daisuke Kawata is also thanked for computing for us predictions of metallicity gradients for galaxies with different masses. We also thanks to the referee, Francesco La Barbera, for his very constructive report, which has help to greatly improve the final version of the manuscript. PS-B also thanks Brad Gibson for his continuing support. GANDALF was developed by the SAURON team and is available from the SAURON website (www.strw.leidenuniv.nl/sauron). This research was supported by a Marie Curie Intra-European Fellowship within the 6th European Community Framework Programme. DAF acknowledges the financial support of the Australian Research Council throughout the course of this work. This work was supported by NSF grant number 0507729.

REFERENCES

Angeletti L., Giannone P., 2003, A&A, 403, 449
Arimoto N., Yoshii Y., 1987, A&A, 173, 23
Barnes J. E., Hernquist L. E., 1991, ApJ, 370, 65
Beasley M. A., Sharples R. M., Bridges T. J., Hanes D. A., Zept S. E., Ashman K. M., Geisler D., 2002, in Geisler D., Grebel E. K., Minniti D., eds, Proc. IAU Symp. 207, Extragalactic Globular Clusters. Astron. Soc. Pac., San Francisco, p. 318
Bekki K., Shioya Y., 1997, ApJ, 478, 17
Bekki K., Shioya Y., 1998, ApJ, 497, 108
Bekki K., Shioya Y., 1999, ApJ, 513, 108
Bell E. F. et al., 2004, ApJ, 608, 752
Bell E. F. et al., 2006, ApJ, 640, 241
Bender R., 1990, A&A, 229, 441
Bender R., Surma P., 1995, A&A, 258, 250
Bender R., Surma P., Doebereiner S., Moellenhoff C., Madejsky R., 1989, A&A, 217, 35
Bender R., Burstein D., Faber S. M., 1992, ApJ, 399, 462
Bendo G. J., Barnes J. E., 2000, MNRAS, 316, 315
Bernardi M., Nichol R. C., Shet R. K., Miller C. J., Brinkmann J., 2006, ApJ, 131, 3
Biller B. A. J. C., Forman W. R., Kraft R., Ensslin T., 2004, ApJ, 613, 238
Binney J., 2004, MNRAS, 347, 1093
Brodie J. P., Strader J., 2006, ARA&A, 44, 193
Brown R. J. N., Forbes D., Kissler-Patig M., Brodie J. P., 2000, MNRAS, 317, 406
Bruzual G., 1983, ApJ, 273, 105

Burstein D., Davies R. L., Dressler A., Faber S. M., Stone R. P. S., Lynden-Bell D., Terlevich R. J., Wegner G., 1987, ApJS, 64, 601
Busarello G., Capaccioli M., D'Onofrio M., Longo G., Richter G., Zaggia S., 1996, A&A, 314, 32
Caldwell N., Rose J. A., Concannon K. D., 2003, AJ, 125, 2891
Cardiel N., 1999, PhD thesis, Universidad Complutense de Madrid
Cardiel N., Gorgas J., Aragón-Salamanca A., 1995, MNRAS, 277, 502
Cardiel N., Gorgas J., Cenarro S., Gonzalez J. J., 1998, A&AS, 127, 597
Carlberg R. G., 1984, ApJ, 286, 403
Carollo C. M., Dazinger I. J., Buson L., 1993, MNRAS, 265, 553
Cattaneo A., Dekel A., Devriendt J., Guiderdoni B., Blaizot J., 2006, MNRAS, 370, 1651
Chiappini C., Matteucci F., Gratton R., 1997, ApJ, 477, 765
Cimatti A., Daddi E., Renzini A., 2006, A&A, 453, 29
Cohen J. G., 1979, ApJ, 228, 405
Cole S., Lacey C. G., Baugh C. M., Frenk C. S., 2000, MNRAS, 319, 168
Davidge T. J., 1991, AJ, 102, 896
Davidge T. J., 1992, AJ, 103, 1512
Davies R. L., Sadler E. M., Peletier R. F., 1993, MNRAS, 262, 650
Dekel A., Birnboim Y., 2006, MNRAS, 368, 2
de Lucia G., Springel V., White S. D. M., Croton D., Kauffmann G., 2006, MNRAS, 366, 499
Denicoló G., Terlevich R., Terlevich E., Forbes D. A., Terlevich A., 2005, MNRAS, 358, 813
de Propris R., Colless M., Driver S. P., Pracy M. B., Couch W. J., 2005, MNRAS, 357, 590
Di Matteo T., Springel V., Hernquist L., 2005, Nat, 433, 604
di Serego Alighieri S. et al., 2005, A&A, 442, 125
Edmunds M. G., Greenhow R. M., 1995, MNRAS, 272, 241
Eggen O. J., Lynden-Bell D., Sandage A. R., 1962, ApJ, 136, 748
Emsellem E. et al., 2004, MNRAS, 352, 721
Faber S. M., Worthey G., González J. J., 1992, in Barbuy B., Renzini A., eds, Proc. IAU Symp. 149, The Stellar Populations of Galaxies. Kluwer, Dordrecht, p. 255
Faber S. M. et al., 1997, AJ, 114, 1771
Faber S. M. et al., 2005, preprint (astro-ph/0506044)
Ferreras I., Charlot S., Silk J., 1999, ApJ, 521, 81
Fisher D., Franx M., Illingworth G., 1995, ApJ, 448, 119
Fisher D., Franx M., Illingworth G., 1996, ApJ, 459, 110
Franx M., 1988, PhD thesis, Rijksuniversiteit
Franx M., Illingworth G. D., 1988, ApJ, 327, 55
Franx M., Illingworth G., 1990, ApJ, 359, 41
Franx M., Illingworth G., Heckman T., 1989, AJ, 98, 538
Fritz A., Ziegler B. L., Bower R. G., Smail I., Davies R. L., 2005, MNRAS, 358, 233
García A. M., 1993, A&AS, 100, 47
Gebhardt K. et al., 2000, AJ, 119, 1157
Gebhardt K. et al., 2003, ApJ, 597, 239
Gibson B. K., 1997, MNRAS, 290, 471
Gibson B. K., Sánchez-Blázquez P., Courty S., Kawata D., 2007, preprint (astro-ph/0611086)
González J. J., 1993, PhD thesis, Univ. Santa Cruz
González J. J., Gorgas J., 1995, in Buzzoni A., Renzini A., Serrano A., eds, ASP Conf. Ser. Vol. 86, Fresh Views of Elliptical Galaxies. Astron. Soc. Pac., San Francisco, p. 225
Gorgas J., Efstathiou G., Aragón-Salamanca A., 1990, MNRAS, 245, 217
Gorgas J., Faber S. M., Burstein D., Gonzalez J. J., Courteau S., Prosser C., 1993, ApJS, 86, 153
Governato F., Reduzzi L., Rampazzo R., 1993, MNRAS, 261, 379
Granato G. L., de Zotti G., Silva L., Bressan A., Danese L., 2004, ApJ, 600, 580
Halliday C., Davies R. L., Kuntschner H., Birkinshaw M., Bender R., Saglia R. P., Baggley G., 2001, MNRAS, 326, 473
Hau G. K. T., Carter D., Balcells M., 1999, MNRAS, 306, 437
Hernquist L., Barnes J. E., 1991, Nat, 254, 210
Heyl J. S., Hernquist L., Spergel D. N., 1994, ApJ, 427, 165
Hinkley S., Im M., 2001, ApJ, 560, 41
Holden B. P. et al., 2005, ApJ, 626, 809
Houdashelt M. L., Trager S. C., Worthey G., Bell R. A., 2002, BAAS, 34, 1118
Idiart T. P., Michard R., de Freitas Pacheco J. A., 2002, A&A, 383, 30
Jesseit R., Naab T., Peletier R., Burkert A., 2007, MNRAS, 376, 997
Jørgensen I., 1999, MNRAS, 306, 607
Kauffmann G., Charlot S., 1998, MNRAS, 294, 705
Kauffmann G. et al., 2003, MNRAS, 341, 54
Kawata D., Gibson B., 2005, MNRAS, 358, 16
Kelson D., Illingworth G. D., van Dokkum P. G., Franx M., 2000, ApJ, 531, 194
Kelson D., Illingworth G. D., Franx M., van Dokkum P. G., 2006, ApJ, 653, 159
Khochfar S., Burkert A., 2003, ApJ, 597, 117
Kobayashi C., 2004, MNRAS, 347, 740
Kobayashi C., Arimoto N., 1999, ApJ, 527, 573
Kodama T., Arimoto N., 1997, A&A, 320, 41
Koeppen J., 1994, A&A, 291, 26
Kormendy J., 1984, ApJ, 287, 577
Kormendy J., Bender R., 1996, ApJ, 464, 119
Kormendy J., Djorgovski S., 1989, ARA&A, 27, 235
Korn A. J., Maraston C., Thomas D., 2005, A&A, 438, 685
Kuntschner H., 2000, MNRAS, 315, 184
Kuntschner H. et al., 2006, MNRAS, 369, 497
La Barbera F., Merluzzi P., Busarello G., Massarotti M., Mercurio A., 2004, A&A, 425, 797
La Barbera F., de Carvalho R. R., Cal R. R., Busarello G., Merluzzi P., Capaccioli M., Djorgovski S. G., 2005, ApJ, 626, 19
Lacey C. G., Fall S. M., 1985, ApJ, 290, 154
Larson R. B., 1974a, MNRAS, 166, 585
Larson R. B., 1974b, MNRAS, 169, 229
Larson R. B., 1975, MNRAS, 173, 671
Lauer T. R. et al., 1995, AJ, 110, 2622
Lauer T. R. et al., 2005, AJ, 129, 2138
Lecureur A., Hill V., Zoccali M., Barbuy B., Gómez A., Minniti D., Ortolani S., Renzini A., 2007, A&A, in press (astro-ph/0610346)
Lima-Neto G. B., Combes F., 1995, A&A, 294, 657
Macchetto F., Pastoriza M., Caon N., Sparks W. B., Giavalisco M., Bender R., Capaccioli M., 1996, A&AS, 120, 463
Martinelli A., Matteucci F., Colafrancesco S., 1998, MNRAS, 298, 42
Mathews W. G., Baker J. C., 1971, ApJ, 170, 241
Matthias M., Gerhard O., 1999, MNRAS, 310, 879
Mehlert D., Thomas D., Saglia R. P., Bender R., Wegner G., 2003, A&A, 407, 423
Menanteau F. et al., 2004, ApJ, 612, 2002
Méndez R. H., Thomas D., Saglia R. P., Maraston C., Kudritzki R. P., Bender R., 2005, ApJ, 627, 767
Meza A., Navarro J. F., Steinmetz M., Eke V. R., 2003, ApJ, 590, 619
Michard R., 1985, A&AS, 59, 205
Michard R., 2005, A&A, 429, 819
Michard R., Prugniel P., 2004, A&A, 423, 833
Mihos J. C., Hernquist L., 1994, ApJ, 437, 47
Morelli L. et al., 2004, MNRAS, 354, 753
Naab T., Jesseit R., Burkert A., 2006a, MNRAS, 372, 839
Naab T., Khochfar S., Burkert A., 2006b, ApJ, 636, L81
Nelan J. E., Smith R. J., Hudson M., Wegner G. A., Lucey J. R., Moore S. A. W., Quinney S. J., Suntzeff N. B., 2005, ApJ, 632, 137
Ocvirk P., Pichon C., Lanọn A., Thiébaut E., 2006a, MNRAS, 365, 46
Ocvirk P., Pichon C., Lanọn A., Thiébaut E., 2006b, MNRAS, 365, 74
Oke J. B. et al., 1995, PASP, 107, 375
Oñorbe J., Domínguez-Tenreiro R., Sáiz A., Serna A., Artal H., 2005, ApJ, 632, 57
Panter B., Heavens A. F., Jimenez R., 2003, MNRAS, 343, 1145
Pedraz S., Gorgas J., Cardiel N., Sánchez-Blázquez P., Guzmán R., 2002, MNRAS, 332, 59
Peletier R. F., Lauberts A., Valentijn E. A., 1989, A&AS, 77, 339
Peletier R. F., Davies R. L., Illingworth G. D., Davies R. L., Illingworth G. D., Davis L. E., Cawson M., 1990, AJ, 100, 1091
Pierce M. et al., 2006, MNRAS, 366, 1253

Pinkney J. et al., 2003, ApJ, 596, 903
Pipino A., Matteucci F., 2006, MNRAS, 365, 1114
Pipino A., Matteucci F., Chiappini C., 2006, ApJ, 638, 739
Proctor R. N., Sansom A. E., 2002, MNRAS, 333, 517
Proctor R. N., Forbes D. A., Hau G. K. T., Beasley M. A., De Silva G. M., Contreras R., Terlevich A. I., 2004a, MNRAS, 349, 1381
Proctor R. N., Forbes D. A., Beasley M. A., 2004b, MNRAS, 355, 1327
Proctor R. N., Forbes D. A., Forestell A., Gebhardt K., 2005, MNRAS, 362, 857
Prugniel P., Nieto J.-L., Simien F., 1987, A&A, 173, 49
Ravindranath S., Ho L. C., Peng C. Y., Filippenko A. V., Sargent W. L. W., 2001, AJ, 122, 653
Reda F., Forbes A. F., Beasley M. A., O'Sullivan E. J., Goudfrooij P., 2004, MNRAS, 354, 851
Rest A., van den Bosch F. C., Jaffe W., Tran H., Tsvetanov Z., Ford H. C., Davies J., Scafer J., 2001, AJ, 121, 2431
Saglia R. P., Maraston C., Greggio L., Bender R., Ziegler B., 2000, A&A, 360, 911
Salpeter E. E., 1955, ApJ, 121, 161
Sánchez-Blázquez P., 2004, PhD thesis, Universidad Complutense de Madrid (PSB04)
Sánchez-Blázquez P. et al., 2006a, MNRAS, 371, 703
Sánchez-Blázquez P., Gorgas J., Cardiel N., González J. J., 2006b, A&A, 457, 787
Sánchez-Blázquez P., Gorgas J., Cardiel N., González J. J., 2006c, A&A, 457, 809
Sánchez-Blázquez P., Gorgas J., Cardiel N., 2006d, A&A, 457, 823
Sargent W. L., Schechter P. L., Boksenberg A., Shortridge K., 1977, ApJ, 212, 326
Sarzi M. et al., 2006, MNRAS, 366, 1151
Savage B. D., Mathis J. S., 1979, ARA&A, 17, 73
Schawinski K. et al., 2006, Nat, 442, 888
Schiavon R. P., 2006, ApJS, in press (astro-ph/0611464)
Schweizer F., Seitzer P., 1992, AJ, 104, 1039
Serra P., Trager S. C., 2007, MNRAS, 374, 769
Sil'chenko O. K., Moiseev A. V., Afanasiev V. L., Chavushyan V. H., Valdes J. R., 2003, ApJ, 591, 185
Silva D. R., Bothun G. D., 1998, AJ, 116, 85
Silva D. R., Elston R., 1994, ApJ, 428, 511
Somerville R. S., Primack J. R., 1999, MNRAS, 310, 1087
Spinrad H., Gunn J. E., Taylor B. J., McClure R. D., Young J. W., 1971, ApJ, 164, 11
Springel V., White S. D. M., Tormen G., Kauffmann G., 2001, MNRAS, 328, 726
Statler T. S., Smecker-Hane R., Cecil G. N., 1996, AJ, 111, 1512
Stiavelli M., Londrillo P., Messina A., 1991, MNRAS, 251, 57
Tabor G., Binney J., 1993, MNRAS, 263, 323
Tamura N., Ohta K., 2000, AJ, 120, 533
Tamura N., Ohta K., 2003, AJ, 126, 596
Tamura N., Kobayashi C., Arimoto N., Kodama T., Ohta K., 2000, AJ, 119, 2134
Tantalo R., Chiosi C., Bressan A., 1998, A&A, 333, 419
Terlevich A., Forbes D. A., 2002, MNRAS, 330, 547
Thomas D., 1999, MNRAS, 306, 655
Thomas D., Greggio L., Bender R., 1999, MNRAS, 302, 537
Thomas D., Maraston C., Bender R., 2003, MNRAS, 339, 897 (TMB03)
Thomas D., Maraston C., Korn A., 2004, MNRAS, 351, 19
Thomas D., Maraston C., Bender R., de Oliveira C., 2005, ApJ, 621, 673
Trager S. C., Worthey G., Faber S. M., Burstein D., Gonzalez J. J., 1998, ApJS, 116, 1
Trager S. C., Faber S. M., Worthey G., González J. J., 2000a, AJ, 119, 1645 (T00a)
Trager S. C., Faber S. M., Worthey G., González J. J., 2000b, AJ, 120, 165
Tran K. H., van Dokkum P., Franx M., Illingworth G. D., Kelson D., Schreiber N. M. F., 2005, ApJ, 627, 25
Tripicco M. J., Bell R. A., 1995, AJ, 110, 3035
Tsujimoto T., Nomoto K., Yoshii Y., Hashimoto M., Yanagida S., Thielemann F. K., 1995, MNRAS, 277, 945
Tucker W., David L., 1997, ApJ, 484, 602
Vader J. P., Vigroux L., Lachieze-Rey M., Souviron J., 1988, A&A, 203, 217
van der Wel A., Franx M., van Dokkum P. G., Rix H. W., Illingworth G. D., Rosati P., 2005, ApJ, 631, 145
van Dokkum P. G., Franx M., 1995, AJ, 110, 2027
van Dokkum P. G., Franx M., Fabricant D., Kelson D. D., Illingworth G. D., 1999, ApJ, 520, 95
Vazdekis A., Kuntschner H., Davies R. L., Arimoto N., Nakamura O., Peletier R., 2001, ApJ, 551, L127
Weil M. L., 1995, PhD thesis, Univ. California, Santa Cruz
White S. D. M., 1980, MNRAS, 191, 1
White S. D. M., Frenk C. S., 1991, ApJ, 379, 52
Whitmore B. C., Miller B. W., Schweizer F., Fall S. M., 1997, AJ, 114, 1797
Worthey G., 1994, ApJS, 95, 107
Worthey G., 1998, PASP, 110, 888
Worthey G., 2004, AJ, 128, 2826
Worthey G., Ottaviani D. L., 1997, ApJS, 111, 377
Worthey G., Faber S. M., González J. J., 1992, ApJ, 398, 69
Worthey G., Faber S. M., González J. J., Burstein D., 1994, ApJS, 94, 687
Wu H., Shao Z., Mo H. J., Xia X., Deng Z., 2005, ApJ, 622, 244
Yamada Y., Arimoto N., Vazdekis A., Peletier R. F., 2006, ApJ, 637, 200

APPENDIX A: PROPERTIES OF INDIVIDUAL GALAXIES

NGC 1600: this galaxy is a X-bright field elliptical E3 galaxy. It does not show any sign of morphological disturbances (Michard & Prugniel 2004). The shape of the isophotes is boxy and has a core shaped inner profile (Bender et al. 1989; Faber et al. 1997). This galaxy has been proposed as a prototype of a merger where the effects of gas have not been very important (Matthias & Gerhard 1999).

NGC 1700: this galaxy shows clear optical signatures of a past merger, including shells and prominent boxiness (Franx et al. 1989; Whitmore et al. 1997; Brown et al. 2000; Lauer et al. 2005). Photometric fine structure at large radii (Schweizer & Seitzer 1992) is also indicative of a merger, a velocity reversal $\sim$50 arcsec northeast suggest a major event. This galaxy shows a counter-rotating core in its centre, but radially increasing prograde rotating in the main body of the galaxy implies that this was not the same event responsible for the counter-rotating core (Statler et al. 1996). The strong rotation at large radius and the nearly oblate shape are consistent with *N*-body simulations of group mergers (Weil 1995). The disturbances are compatible with a merger of three or more stellar systems 2–4 Gyr ago. Despite this process, this galaxy follow the same Mg–σ relation that the rest of elliptical galaxies (e.g. T00a; Sánchez-Blázquez et al. 2006b). NGC 1700 is situated in an small group of galaxies with three members (García 1993).

NGC 2865: this galaxy also shows strong morphological peculiarities ($\sigma_2 = 10.6$; Michard 2005), which can be indicative of recent interactions. It also shows very young mean age in its centre (Hau et al. 1999; Michard 2005, see Section 6).

NGC 3377: this galaxy, situated in the Leo I group, shows presence of dust (Lauer et al. 2005) and a stellar disc. The galaxy has discy isophotes in the inner regions, but boxy in the outer regions (Peletier et al. 1990), and it has a *power-law* central luminosity profile (Faber et al. 1997; Rest et al. 2001).

NGC 3779: this galaxy, from the Leo I group, does not show any sign of morphological disturbance (Schweizer & Seitzer 1992). There is, however, a small nuclear dust ring (van Dokkum & Franx 1995; Lauer et al. 2005), and some ionized gas that extends to a radius of 8 arcsec (Macchetto et al. 1996). All the globular clusters

seem to be old and show a broad dispersion in metallicity (Pierce et al. 2006). The dynamics of this galaxy is explained assuming a merger where the gas dissipation has not been important (Gebhardt et al. 2000).

NGC 3384: the galaxy, also from the Leo I group, is the only S0 of our sample. It shows a circumnuclear disc (Sil'chenko et al. 2003) and a disc or a secondary bar aligned with the major axis. This galaxy also has a non-symmetric distribution of stars in the disc (Busarello et al. 1996). NGC 3384 has been proposed as a candidate for a pseudo-bulge (Pinkney et al. 2003).

NGC 4387: this Virgo galaxy shows and old central age ($\sim$12.5 Gyr; Sánchez-Blázquez et al. 2006c; Yamada et al. 2006. It is a boxy galaxy and it shows a central velocity dispersion drop (Halliday et al. 2001; Emsellem et al. 2004). This decrease in σ in the central parts of galaxies is predicted for remnants of an equal-mass merger of two spirals (Bendo & Barnes 2000).

NGC 4458: this low luminosity galaxy, situated in the Virgo cluster, also shows a nuclear stellar disc consistent with the presence of a central fast-rotating component in the stellar velocity field (Morelli et al. 2004) and a hot kinematically decoupled core. The cold central disc of NGC 4458 does not show any difference in terms of stellar population with the main body of the galaxy (Morelli et al. 2004). The galaxy shows deviations from the $r^{1/4}$ law in their outskirts (Michard 1985; Prugniel, Nieto & Simien 1987; Peletier et al. 1990), which have been explained as a result of tidal interaction with NGC 4461 and 4486.

NGC 4464: this galaxy, situated in the Virgo cluster, shows a power-law inner profile (Faber et al. 1997; Lauer et al. 2005).

NGC 4472: this giant elliptical, situated in the Virgo cluster, has X-ray holes or cavities within radii of $\sim$2 kpc which may have been produced during a period of nuclear activity that began 1.2×10^7 yr ago and may be ongoing (Biller et al. 2004). The globular clusters of this galaxy seem to be old and coeval but they show a range in metallicity from $-1.6 <$ [Fe/H] < 0 dex (Beasley et al. 2002).

NGC 4551: this galaxy, one of the members of the Virgo cluster, presents a power-law inner profile (Faber et al. 1997; Lauer et al. 2005). A central decrease in the velocity dispersion has been also found (Halliday et al. 2001).

APPENDIX B: TRANSFORMATION TO THE LICK SYSTEM

In Fig. B1 a comparison between the original Lick/IDS index measurements of galaxies in common with our data is shown. Indices in the Lick/IDS galaxies have been measured within an aperture of 4×1.5 arcsec^2 (Trager et al. 1998) while we tried to match this aperture extracting the spectra within the central 4 arcsec. Therefore, obtaining an aperture of 4×2 arcsec^2. Fig. B2 shows the comparison between the fully calibrated data by Sánchez-Blázquez (2004) and this work. We selected, from the first study, the measurements within an aperture of 1.4×4 arcsec^2.

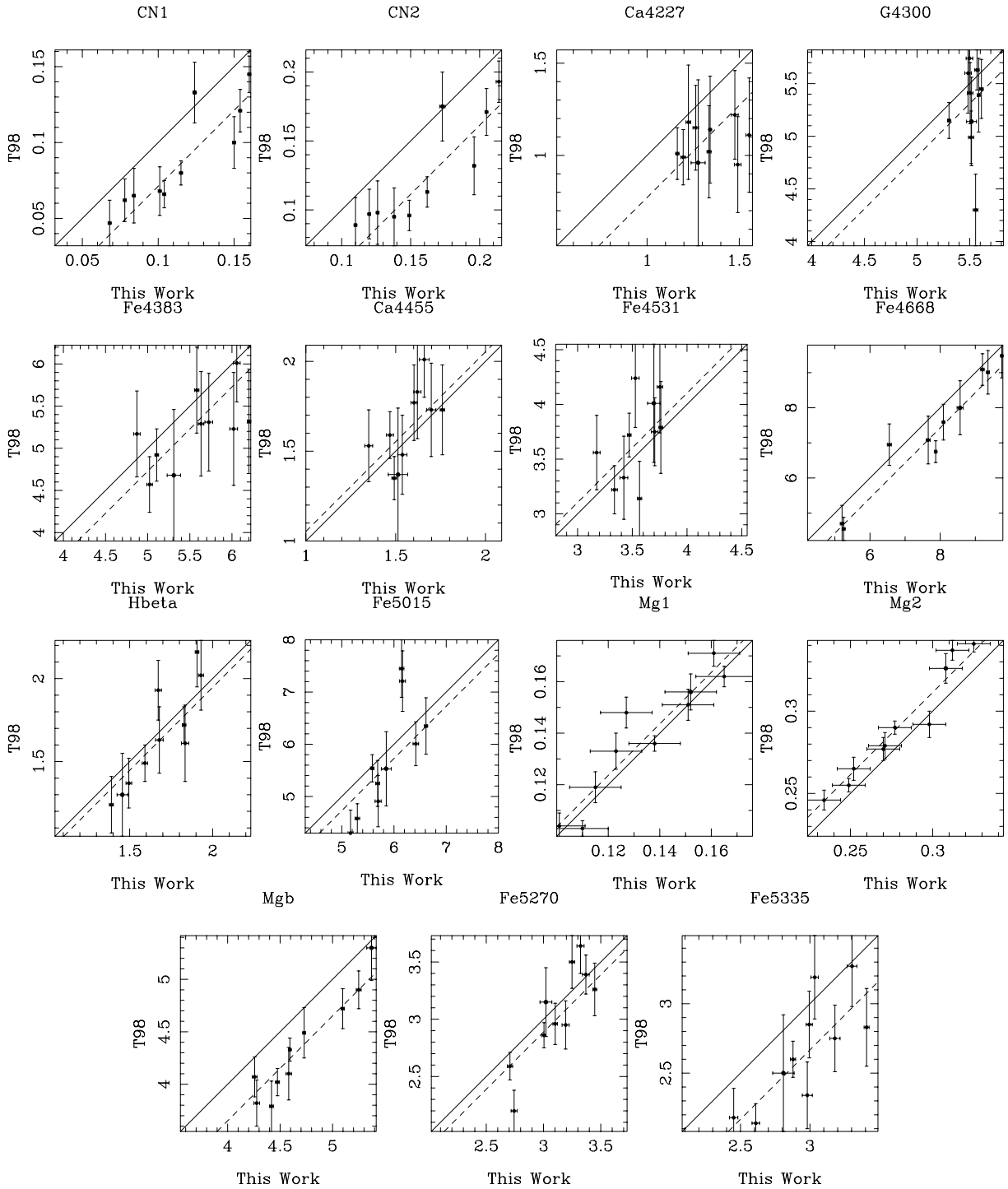

Figure B1. Comparison of the line-strength indices for the galaxies in common between Trager et al. (1998) (T98) and this study. Solid line shows the 1:1 line while the dashed line shows the calculated mean offset between both samples (see text for details.

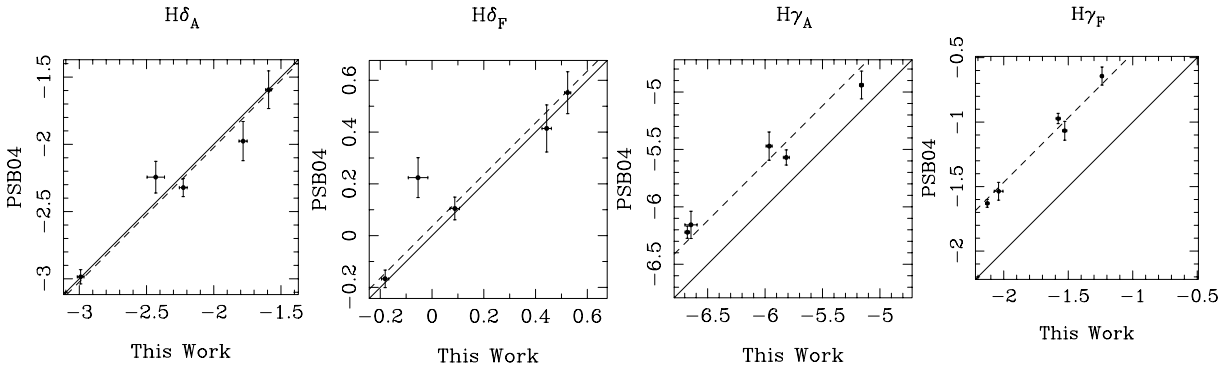

Figure B2. Comparison of the line-strength indices for the galaxies in common with Sánchez-Blázquez (2004; hereafter PSB04) and this study. Solid line shows the 1:1 relation while the dashed line shows the mean offset between samples (see text for details).

APPENDIX C: COMPARISON WITH OTHER STUDIES

Some of the galaxies analysed in this study have been already studied by other authors. In particular, we have five galaxies in common with Kuntschner et al. (2006) and two galaxies in common with Fisher et al. (1996). The data by Kuntschner et al. (2006) were acquired with an Integral Field Unit (SAURON), but the authors kindly provided us with the extracted gradients from their data assuming an slit width and position angle as the one in our study. Figs C1 and C2 show this comparison. In some cases, we have adjusted the zero-point as we are interested in the gradients.

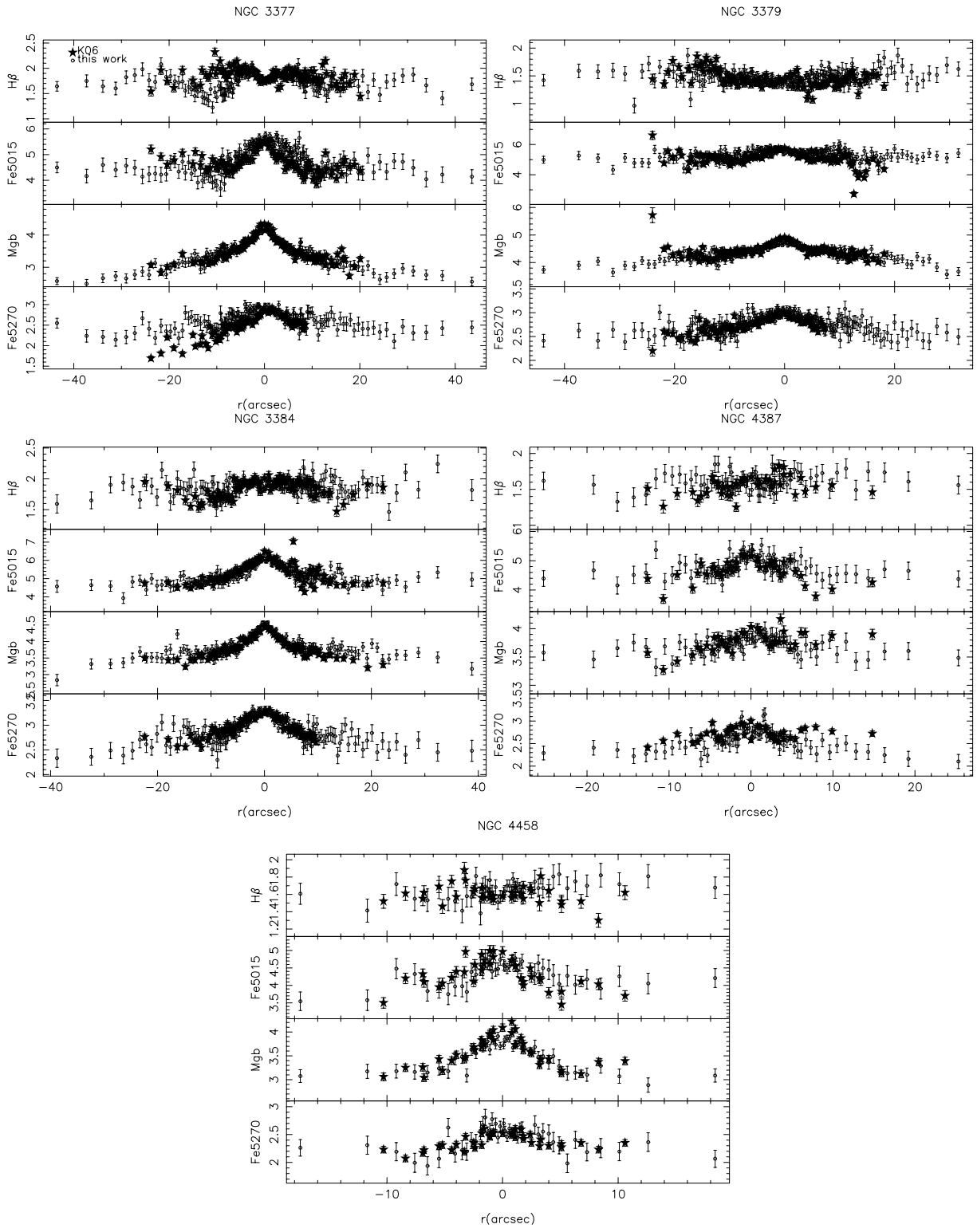

Figure C1. Comparison of the line-strength indices with radius measured in Kuntschner et al. (2006) (stars) and in this work (small open circles).

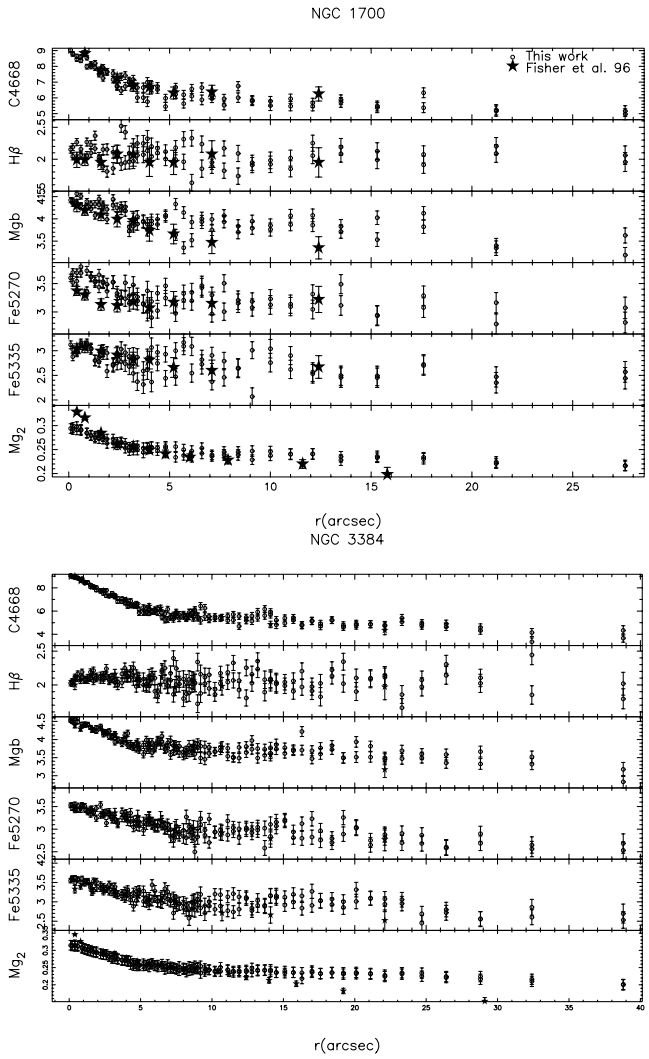

Figure C2. Comparison of the line-strength indices with radius obtained in Fisher et al. (1996) (stars) and in this work (small open circles).

APPENDIX D: CENTRAL LINE-STRENGTH INDICES

Table D1 shows the indices and velocity dispersion measured in the spectra extracted within an aperture of 2 arcsec $\times$ $r_{\rm eff}/8$.

Table D1. Line-strength indices and velocity dispersion within an aperture of 2 arcsec $\times$ $r_{\rm eff}/8$.

Galaxy	σ (km s^{-1})	D4000 (Å)	Hδ_A (Å)	Hδ_F (Å)	CN$_1$ (Å)	CN$_2$ (Å)	Ca4227 (Å)	G4300 (Å)	Hγ_A (Å)	Hγ_F (Å)
NGC 1600	333.0	1.865	−2.444	−0.010	0.122	0.170	1.338	5.446	−6.573	−1.992
	1.6	0.015	0.038	0.022	0.001	0.001	0.021	0.027	0.030	0.019
NGC 1700	177.7	1.993	−1.670	0.475	0.088	0.126	1.220	5.476	−5.840	−1.464
	0.7	0.016	0.025	0.015	0.001	0.001	0.011	0.018	0.021	0.013
NGC 2865	182.8	1.655	2.809	2.504	−0.019	0.030	0.759	3.825	−0.955	1.402
	1.0	0.013	0.023	0.013	0.001	0.001	0.011	0.018	0.019	0.012
NGC 3377	153.2	1.912	−1.415	0.570	0.102	0.149	1.135	5.276	−5.023	−1.166
	0.5	0.015	0.019	0.010	0.001	0.001	0.007	0.012	0.014	0.008
NGC 3379	222.8	1.998	−2.793	−0.131	0.143	0.192	1.339	5.639	−6.593	−2.074
	0.7	0.016	0.020	0.010	0.001	0.001	0.007	0.011	0.013	0.008
NGC 3384	134.1	2.004	−2.609	0.079	0.132	0.177	1.337	5.535	−6.273	−1.742
	0.6	0.016	0.019	0.010	0.001	0.001	0.006	0.011	0.014	0.008
NGC 4387	140.5	1.888	−2.097	0.186	0.052	0.093	1.472	5.434	−5.741	−1.538
	0.7	0.015	0.029	0.018	0.001	0.001	0.012	0.022	0.026	0.016
NGC 4458	112.2	2.048	−1.716	0.311	0.072	0.114	1.271	5.495	−5.285	−1.313
	0.8	0.016	0.033	0.020	0.001	0.001	0.014	0.024	0.029	0.018
NGC 4464	152.3	1.946	−2.224	0.095	0.102	0.147	1.201	5.565	−5.808	−1.583
	0.7	0.016	0.027	0.017	0.001	0.001	0.012	0.020	0.024	0.015
NGC 4472	281.6	1.979	−2.710	−0.161	0.137	0.187	1.390	5.473	−6.609	−1.964
	0.9	0.016	0.022	0.011	0.001	0.001	0.008	0.012	0.014	0.009
NGC 4551	133.4	1.887	−2.058	0.202	0.062	0.104	1.493	5.431	−5.926	−1.581
	0.7	0.015	0.030	0.018	0.001	0.001	0.012	0.022	0.026	0.016

Galaxy	Fe4383 (Å)	Ca4455 (Å)	Fe4531 (Å)	C4668 (Å)	Hβ (Å)	Fe5015 (Å)	Mg$_1$ (mag)	Mg$_2$ (mag)	Mgb (Å)	Fe5270 (Å)	Fe5335 (Å)
NGC 1600	5.395	1.525	3.642	8.468	1.422	5.823	0.149	0.306	5.302	3.040	2.881
	0.043	0.030	0.032	0.051	0.018	0.056	0.010	0.010	0.025	0.031	0.043
NGC 1700	5.568	1.595	3.676	8.906	1.929	5.961	0.121	0.262	4.323	3.151	2.957
	0.028	0.016	0.021	0.037	0.013	0.038	0.010	0.010	0.016	0.021	0.023
NGC 2865	3.785	1.267	3.217	6.194	3.189	5.765	0.072	0.177	3.062	2.703	2.679
	0.028	0.017	0.022	0.038	0.013	0.040	0.009	0.009	0.017	0.021	0.025
NGC 3377	5.049	1.464	3.413	7.597	1.860	5.531	0.134	0.269	4.501	2.976	2.841
	0.018	0.011	0.014	0.029	0.008	0.030	0.010	0.010	0.011	0.016	0.016
NGC 3379	5.522	1.575	3.530	7.961	1.429	5.641	0.157	0.306	5.011	3.057	2.950
	0.018	0.012	0.014	0.029	0.008	0.030	0.010	0.010	0.011	0.016	0.016
NGC 3384	6.040	1.709	3.678	9.252	1.910	6.423	0.144	0.287	4.592	3.371	3.307
	0.017	0.010	0.013	0.028	0.008	0.029	0.010	0.010	0.011	0.015	0.014
NGC 4387	5.455	1.498	3.361	6.025	1.715	5.480	0.109	0.244	4.224	3.028	2.893
	0.032	0.018	0.024	0.043	0.016	0.043	0.010	0.010	0.018	0.023	0.026
NGC 4458	4.855	1.350	3.169	5.154	1.674	5.144	0.100	0.232	4.233	2.730	2.445
	0.036	0.021	0.028	0.048	0.017	0.046	0.010	0.010	0.020	0.024	0.028
NGC 4464	5.015	1.460	3.327	5.225	1.595	5.322	0.109	0.248	4.451	2.714	2.612
	0.030	0.018	0.024	0.042	0.015	0.042	0.010	0.010	0.017	0.022	0.025
NGC 4472	5.675	1.586	3.557	8.424	1.507	6.081	0.157	0.312	5.064	3.129	3.018
	0.020	0.014	0.015	0.030	0.009	0.033	0.011	0.010	0.012	0.018	0.018
NGC 4551	5.691	1.589	3.435	6.845	1.807	5.870	0.114	0.256	4.449	3.150	3.074
	0.032	0.018	0.025	0.042	0.016	0.042	0.010	0.010	0.018	0.023	0.025

This paper has been typeset from a TEX/LATEX file prepared by the author.